TECHNICAL REVIEWS

Computational models for active matter

M. Reza Shaebani[1]✉, *Adam Wysocki*[1], *Roland G. Winkler*[2], *Gerhard Gompper*[2]✉ *and Heiko Rieger*[1]✉

Abstract | Active matter, which ranges from molecular motors to groups of animals, exists at different length scales and timescales, and various computational models have been proposed to describe and predict its behaviour. The diversity of the methods and the challenges in modelling active matter primarily originate from the out-of-equilibrium character, lack of detailed balance and of time-reversal symmetry, multiscale nature, nonlinearity and multibody interactions. Models exist for both dry active matter and active matter in fluids, and can be agent-based or continuum-level descriptions. They can be generic, emphasizing universal features, or detailed, capturing specific features. We compare various modelling approaches and numerical techniques to illuminate the innovations and challenges in understanding active matter.

Active matter consists of particles, agents or constituents that consume energy, which they use to generate directed motion, forces and shape deformations, or even to proliferate and annihilate. Living systems — in which active units reproduce, adapt and dynamically respond to environmental changes — are paradigmatic examples of active matter. Active matter systems are out of equilibrium, and the nature of the energy input distinguishes them from externally driven systems such as shear flow. Some of the basic features of active matter are broken time-reversal symmetry, broken detailed balance and lack of an equation of state. New models, methods and computational techniques have been developed in the past two decades to understand and unravel the emerging physical principles governing active matter[1–5]. Of particular interest are emerging many-particle effects or collective phenomena, such as motility-induced phase separation (MIPS), spontaneous rotational symmetry breaking in two dimensions, pattern formation and self-organization. The diversity of active agents and their wide range of behaviours are major challenges in developing a comprehensive theoretical description of living matter. Various numerical methods with different levels of resolution, ranging from microscale to macroscale, have been developed and used to model active matter[1–5] (FIG. 1). The goal of this Technical Review is to summarize and compare currently available models and to elucidate challenges in computational modelling of active matter.

We first consider dry active matter, that is, systems for which hydrodynamic interactions are absent and momentum is not conserved. Next, approaches for modelling hydrodynamics of active suspensions are discussed. In these approaches, the dynamics of the solvent is incorporated in the model, ensuring local momentum conservation. We also present an overview of the continuum models used for active fluids, and discuss the practical relevance of the numerical approaches. The degree of coarse-graining determines the details of real systems that can be captured, which becomes most evident in the modelling of cells, tissues and animal groups. The different scales of living systems necessitate different model approaches, ranging from all-atom molecular dynamics (MD) simulations for force-generating protein machines, over coarse-grained particle-based models and continuum models, to agent-based models with phenomenological interaction rules. Finally, we address the open challenges faced by researchers modelling active matter and present an outlook on model developments toward real-world applications.

Dry active matter

Dry active systems are characterized by the absence of momentum conservation. This can be due to contact with a momentum-absorbing medium, as in bacteria gliding or granular beads vibrating on frictional surfaces. The omission of momentum conservation may also originate from the minor relevance of hydrodynamic interactions in systems where other effects, such as fluctuations, volume exclusion, and short-range or metric-free interactions, dominate. Relevant examples include animal flocks and dense collections of swimming bacteria. We discuss two paradigmatic minimal models of dry active matter and their variants and extensions: active Brownian particles (ABPs) and Vicsek-type models with alignment interactions. We also briefly address

[1]*Department of Theoretical Physics and Center for Biophysics, Saarland University, Saarbrücken, Germany.*

[2]*Theoretical Soft Matter and Biophysics, Institute of Complex Systems and Institute for Advanced Simulation, Forschungszentrum Jülich, Jülich, Germany.*

✉*e-mail: shaebani@lusi.uni-sb.de; g.gompper@fz-juelich.de; h.rieger@physik.uni-saarland.de*

https://doi.org/10.1038/s42254-020-0152-1

Key points

- Active matter exhibits a wide range of emergent non-equilibrium phenomena, theoretical studies of which often require computer simulations.
- Active matter encompasses synthetic and living systems, including active gels and the cytoskeleton, cells and tissues, nanorobots and microrobots, synthetic and biological microswimmers, and animal herds.
- Active matter is characterized by out-of-equilibrium behaviour, nonlinearity, multibody interactions, lack of detailed balance or time-reversal symmetry and, generically, absence of an equation of state.
- The wide spectrum of systems and phenomena requires a multitude of models and simulation techniques, from agent-based to continuum-level approaches, and combinations thereof.
- Active agents can interact in many ways, such as volume exclusion, contact attraction, visual information and hydrodynamics. Hydrodynamic interactions are ubiquitous for self-propelled particles in an aqueous environment, which implies a classification into dry and wet active matter.

continuum-modelling approaches. Neglecting birth, division and death processes, we consider only systems in which the number of particles is conserved.

Active Brownian particles

A rather generic model of an active agent is the ABP, a self-propelled spherical particle with dynamics described by the overdamped Langevin equations[6,7]

$$\begin{aligned}\frac{\mathrm{d}\boldsymbol{r}(t)}{\mathrm{d}t} &= \frac{D}{k_\mathrm{B}T}[-\nabla U(\boldsymbol{r})+\boldsymbol{F}_\mathrm{active}]+\sqrt{2D}\,\boldsymbol{\xi}(t)\\ \frac{\mathrm{d}\boldsymbol{e}(t)}{\mathrm{d}t} &= \sqrt{2D_\mathrm{r}}\,\hat{\boldsymbol{e}}(t)\times\boldsymbol{\xi}_\mathrm{r}(t)\end{aligned} \quad (1)$$

for the position $\boldsymbol{r}(t)$ and the unit orientation vector $\hat{\boldsymbol{e}}(t)$. D is the translational diffusion coefficient, D_r is the rotational diffusion coefficient, $U(\boldsymbol{r})$ is either the interaction energy with other particles or an external potential, and $\boldsymbol{F}_\mathrm{active}$ is a self-propulsion force (usually along the current direction of motion, that is, $\boldsymbol{F}_\mathrm{active}=F_0\hat{\boldsymbol{e}}$, where F_0 is a constant). k_B is the Boltzmann constant and T is temperature. The uncorrelated white noises $\boldsymbol{\xi}$ and $\boldsymbol{\xi}_\mathrm{r}$ follow a unit normal distribution. The overdamped limit of equation 1 is suitable for modelling motion in low-Reynolds-number fluids, such as in biological environments.

Active particles, even with purely repulsive interactions, exhibit features not seen in ordinary particles, such as MIPS[4,5,8–15], wall accumulation[16–18], capillary action in spite of wall–particle repulsion[19], and an active pressure (denoted as swim pressure)[6,18,20–22]. An intuitive explanation for the separation into dense and dilute regions of ABPs is that there is positive feedback between the blocking of persistent particle motion by steric interactions, and an enhanced probability of collisions with additional particles at sufficiently large concentrations. The reduction in speed by collisions leads to a local increase in density, which further increases the collision frequency in those regions. This mechanism eventually leads to particle accumulation and phase separation. During MIPS, the phase-separated domains grow self-similarly in time and their size is limited only by the system dimensions[10,11]. Remarkably, in 3D, ABPs exhibit collective motion in the high-density phase-separated state even in the absence of an alignment rule[10]. Similarly, wall accumulation emerges by the (slow) orientational diffusion of adsorbed ABPs, which are only able to escape when their propulsion direction points away from the wall[4,16]. The strength of the effects depends on the rotational diffusion coefficient, the propulsion velocity and the curvature of the surface. Simulations show that ABPs accumulate preferentially in regions of highest curvature[17,23]. Although non-equilibrium active systems usually lack a free energy and equations of state, spherical ABPs are a notable exception. Analytical considerations and simulations yield a pressure equation of state in this case[6,18,20–22]; however, such an equation does not exist for non-spherical, elongated ABPs[6].

Extensions of the ABP model include models with additional active torques, models of particles with asymmetric shapes, such as rods and L-shaped microswimmers, and assemblies of several active particles, for instance in a polymer-like manner[24–31]. Such assemblies exhibit unusual emerging effects such as suppression of MIPS and appearance of large-scale coherent motion, chiral motion patterns, and an intimate coupling of activity and polymer conformations and dynamics. Other approaches to simulate self-propelled particle systems include active lattice gas model and (kinetic) Monte Carlo approaches[32–38].

Active motion with alignment interactions

Intriguing common features — such as swirling patterns and swarming — are shared by the collective motion in various systems of living organisms (examples being flocks of birds and animal herds) and ensembles of synthetic elongated active particles. These features are related to the alignment of motion with their neighbours[39].

The Vicsek model is an agent-based minimal model for flocking, accounting for the interplay between fluctuations and simultaneous interactions of multiple agents[40]. Particles moving in a plane with constant velocity modulus v_0 align with their neighbours by updating their velocity angle θ at each time step according to

$$\theta_i(t+1)=\langle\theta_i(t)\rangle_R+\xi_i(t) \quad (2)$$

where $\langle\theta_i(t)\rangle_R$ is the average velocity angle of particles located in a circle of radius R surrounding particle i. $\xi_i(t)$ is a random angle obtained from a uniform distribution $[-\sigma\pi,\sigma\pi]$, such that $\sigma\in[0,1]$ defines the noise strength. The new position of particle i is then given by $\boldsymbol{x}_i(t+1)=\boldsymbol{x}_i(t)+v_0\,\hat{\boldsymbol{e}}_i$, where $\hat{\boldsymbol{e}}_i=(\cos\theta_i(t+1),\sin\theta_i(t+1))$ is the new velocity direction. A continuous transition from disordered to an ordered state occurs on increasing the particle density or decreasing σ. The global mean normalized velocity $m=N^{-1}|\sum_{i=1}^{N}\hat{\boldsymbol{e}}_i|$ is an appropriate order parameter, characterizing the transition from random ($m=0$) to coherent movement ($m=1$). Despite this being a non-equilibrium phase transition, various notions of equilibrium statistical mechanics can be applied to it, owing to spontaneous symmetry breaking and the emergence of well-defined macroscopic states.

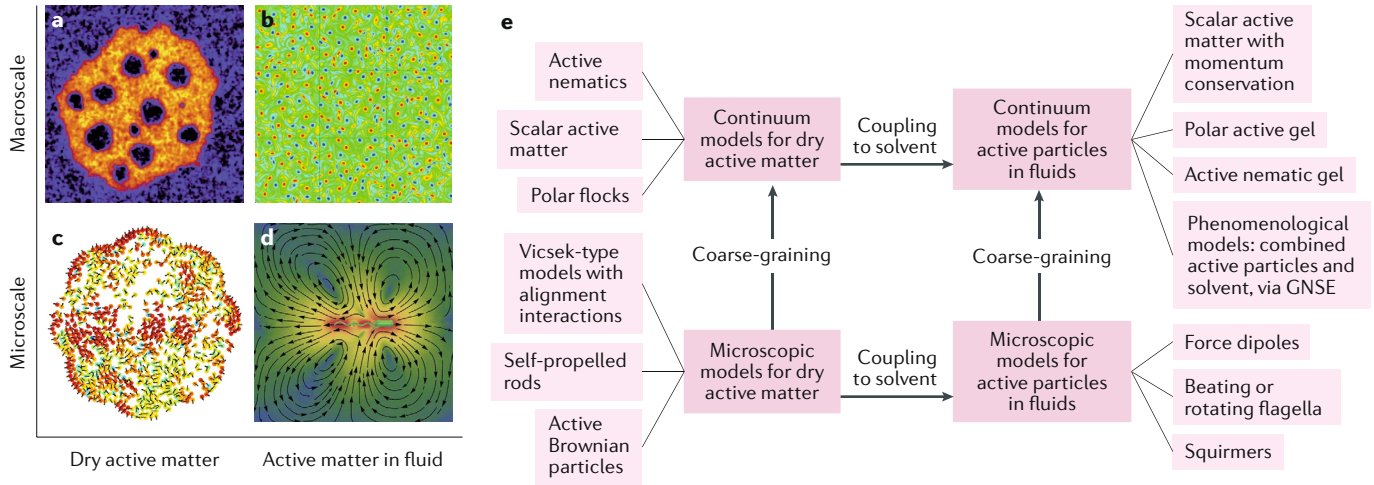

Fig. 1 | **Modelling active matter. a–d** | Typical snapshots of numerical simulations of active systems in (dry–wet, micro–macro) phase space. **a** | Bubbly phase separation in the density profile of a continuum dry active-matter model. 'Boiling liquid' phase is indicated in yellow; 'vapour' phase is indicated in blue. **b** | Vorticity field in the turbulent regime of a continuum active fluid model. **c** | Ordering of vibrated polar disks in confinement. Colour denotes the relative alignment of dry active particles to their neighbours, ranging from blue (antiparallel) to red (parallel). **d** | Flow field generated by a single swimming bacterium. **e** | The main computational models and methods for active matter. GNSE, generalized Navier–Stokes equations. Panel **a** is adapted from REF.[70], CC-BY-4.00 (https://creativecommons.org/licenses/by/4.0/). Panel **b** is adapted with permission from REF.[291], PNAS. Panel **c** is adapted with permission from REF.[292], APS. Panel **d** is adapted from REF.[112], CC-BY-3.00 (https://creativecommons.org/licenses/by/3.0/).

The flocking transition in the Vicsek model is reminiscent of a liquid–gas transition, rather than an order–disorder transition, but with microphase separation in the coexistence region, where travelling ordered bands of finite width coexist with a disordered gas[41]. By contrast, the corresponding lattice model, called the active Ising model, exhibits full phase separation[42]. As established in many studies[39], the patterns in a system described by the Vicsek model, such as band formation[43,44], rotating chains[45] and marching groups, and the essential characteristics of collective motion, such as the nature of the phase transition, are influenced by several factors. These factors include how noise and disorder are introduced into the system[46–48], boundary conditions (which can be periodic or reflecting, and can take different shapes)[49], the range[50] and type of interactions (including hard core, metric-free, repulsive or attractive)[44,51–53] and alignment rules (for example, polar or bipolar)[54–56]. For example, the order of the transition depends on whether the noise is intrinsic (perturbing the final orientation) or extrinsic (perturbing the individual orientations before averaging)[46,47]; whether interactions are metric (occur over a fixed range) or topological (occur between a fixed number of partners)[52]; and the magnitude of the particle displacement $v_0\Delta t$ during one time step compared with the radius of interaction (R)[50]. Furthermore, alignment can be introduced in several ways. In animal herds, agents sense the motion of their neighbours, resulting in polar alignment. However, an explicit (polar) alignment rule is not necessary for coherent motion: the alignment can be induced implicitly through purely physical local interactions such as inelastic[49] or nematic collisions[43], short-range interactions[45,57] or volume exclusion in combination with shape-induced (particle elongation) effects[58]. An important question is the minimal requirements for emerging collective motion by solely physical interactions. FIGURE 2 lists some variants of the Vicsek model and a few systems that show collective motion without explicit alignment rules.

Continuum models of dry active matter

The large-scale behaviour of many-particle systems can be captured by continuum models, which describe the evolution of continuous slow variables such as number-density $n(\boldsymbol{r},t)$ and velocity $\boldsymbol{v}(\boldsymbol{r},t)$ fields. Macroscopic approaches capture the main features of active matter, such as collective motion, by considering the conservation laws and broken continuous symmetries. Continuum theories can be constructed by coarse-graining a microscopic model, adopting symmetry arguments or using out-of-equilibrium thermodynamics close to equilibrium. Representative continuum models of dry active matter, which conserve the number of particles without conserving momentum, are provided in TABLE 1.

Dry polar flocks. The first continuum description of the Vicsek model, solely based on symmetry considerations, is the Toner–Tu model[3,59–62]. The theory describes active particles that have the front distinguished from the rear and, therefore, are characterized by a polarization field $\boldsymbol{p}(\boldsymbol{r},t)$ corresponding to the vectorial orientation of active particles and their direction of swimming. The conservation of the number density, $n(\boldsymbol{r},t)$, results in a continuity equation that includes an active contribution $v_0 n\,\boldsymbol{p}$ to the particle flux (see equation 6 in TABLE 1). The simplest form of the dynamical equation for $\boldsymbol{p}$ assumes a relaxation process toward the minimum of an effective free energy $\mathcal{F}[n,\boldsymbol{p}]$, which includes terms responsible for the spontaneous polarization and the energetic

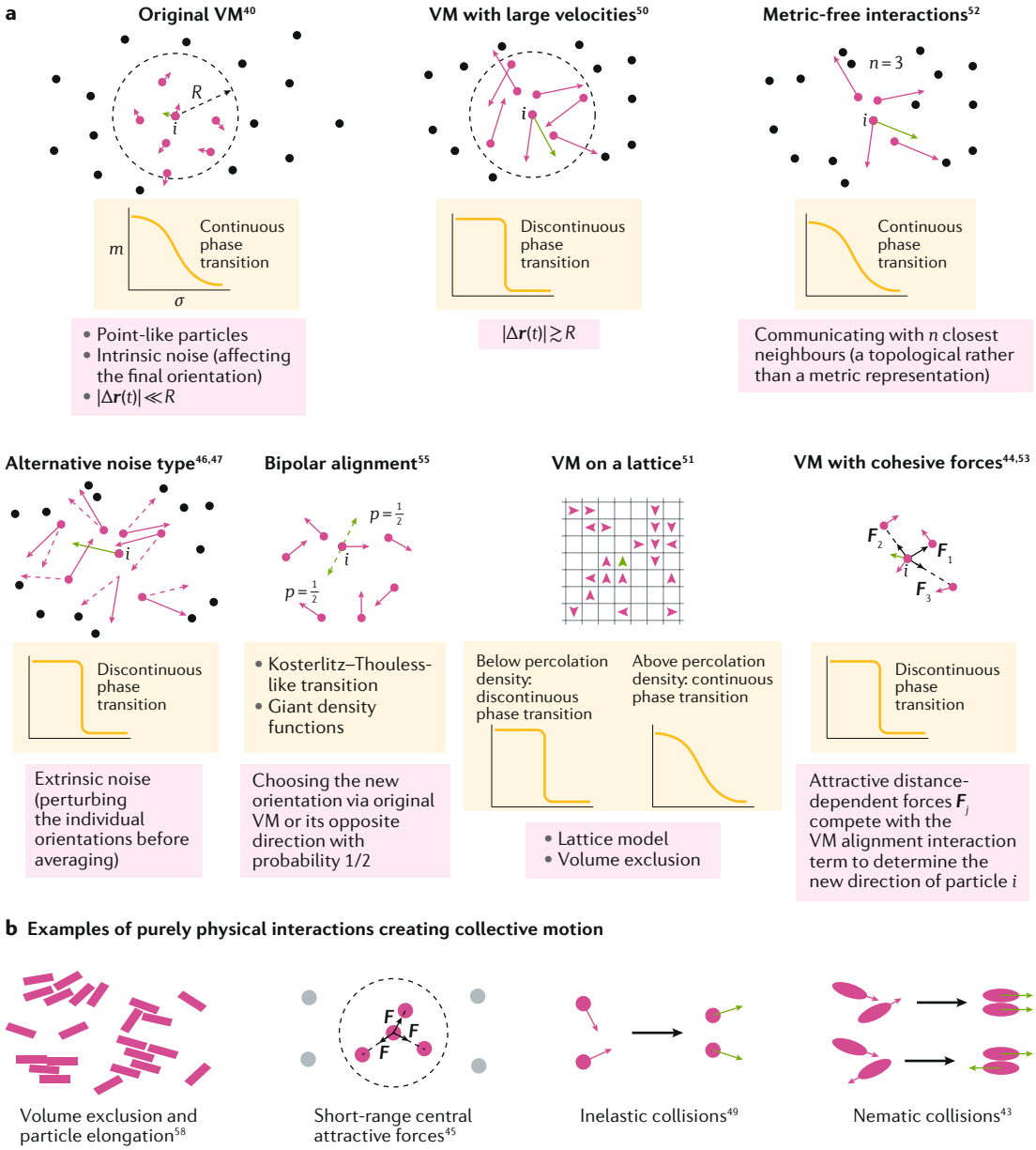

Fig. 2 | **Models of dry active matter. a** | Variants of the Vicsek model (VM). Green vectors indicate the orientation adopted by the central particle *i*. Purple arrows are the directions that enter in the calculation for the new direction of particle *i*. **b** | Examples of purely physical interactions that create collective motion. σ, noise strength; m, order parameter; R, radius of interaction; $\Delta\boldsymbol{r}(t)$, particle displacement during one time step; $\boldsymbol{F}$, force; p, probability.

cost of elastic distortions of the orientational field. As shown in equation 7, activity enters solely via an advective term $\lambda(\boldsymbol{p}\cdot\nabla)\boldsymbol{p}$ (λ is the coefficient of convective derivative), which accounts for the fact that distortions in $\boldsymbol{p}$ are advected by itself because $\boldsymbol{p}$ represents both the order parameter and the velocity. Flocks do not conserve momentum, and the system lacks Galilean invariance; therefore, $\lambda \neq v_0$, meaning that density and polarization inhomogeneities advect at different velocities. The model exhibits giant number fluctuations and long-range order in 2D (forbidden in thermal equilibrium by the Mermin–Wagner theorem)[3,59]. By relaxing the constraint on number-density conservation, the model can be generalized and applied to systems involving birth–division–death processes[63] such as in dense bacterial colonies.

Dry active nematics. A system of apolar (that is, head–tail symmetric) active particles can exhibit a state that has long-range directional order, but with zero global drift velocity because of the nematic symmetry. Active nematics can be characterized by a symmetric second-rank tensor $\boldsymbol{Q}(\boldsymbol{r},t)$, which represents the local alignment of neighbouring particles (equation 8). The overdamped dynamics of $\boldsymbol{Q}$ obeys equation 9, which reduces to the free energy $\mathcal{F}[n,\boldsymbol{Q}]$ consisting of entirely quasi-passive terms. The continuity equation 10 for the density $n(\boldsymbol{r},t)$ contains an active current $\boldsymbol{J}_{\text{active}} = \zeta\nabla\cdot\boldsymbol{Q}$ (REFS[64,65]),

originating from the force dipole of active particles (ζ is the coefficient of active current). $\boldsymbol{J}_{\text{active}}$ accounts for particle flux along or against the curvature $\nabla \cdot \boldsymbol{Q}$, thus violating time-reversal symmetry. Despite the simplicity of the model, active nematics exhibit interesting behaviour, such as giant number fluctuations and self-propulsion of topological defects[1,64,65]. An extension to a more complex environment, such as viscoelasticity by polymers[66], implies additional effects, such as drag reduction, spontaneous flows caused by an antagonistic coupling between polymer and nematic orientations, and active turbulence in a sufficiently soft elastomeric solid[67].

Dry scalar active matter. Anisotropic interactions are responsible for orientational order–disorder transitions in active nematics or polar matter. In contrast, active particles with spherical symmetry (that is, without alignment interactions) do not display a global directional order ($\boldsymbol{p} = \boldsymbol{Q} = 0$), and the only remaining slow variable is the scalar number density n. To explore the physics of MIPS in scalar active matter, the passive model B[68] — a field-theoretical model for diffusive phase separation of the number density, characterized by a conserved scalar order parameter ϕ — has been extended by an active chemical potential $\mu_{\text{active}} = \lambda(\nabla\phi)^2$ that breaks the time-reversal symmetry at leading order in the density gradient expansion[69–73]. To allow for circulating real-space particle currents in steady state, further terms that break the gradient structure of the active current have been added[70] (see equations 11 and 12 in TABLE 1). The resulting active model B+ (AMB+) displays complex dynamics such as microphase separation (bubbles of a finite length scale) and a reverse Ostwald process (increase of the number of small bubbles while bigger bubbles evaporate)[70].

Active particles in fluids

Hydrodynamic interactions are fundamental for active particles immersed in a fluid, and determine their behaviour in various respects. On the one hand, they are an integral part of the propulsion system of most biological and synthetic microswimmers — without

Table 1 | **The governing equations of continuum models for dry active matter and active particles in fluids**

Continuum model	Governing equations	Parameters
Dry active matter		
Toner–Tu model[59,60] (dry polar flocks)	$\partial_t n + \nabla \cdot (v_0 n\boldsymbol{p} + \boldsymbol{J}_{\text{passive}}) = 0$ (6) $\partial_t \boldsymbol{p} + \lambda(\boldsymbol{p}\cdot\nabla)\boldsymbol{p} + \ldots = -\Gamma_r \frac{\delta \mathcal{F}[n,\boldsymbol{p}]}{\delta \boldsymbol{p}} + \boldsymbol{\chi}$ (7)	v_0, propulsion speed; λ, coefficient of convective derivative; $\boldsymbol{J}_{\text{passive}}$, particle flux; $\boldsymbol{\chi}$, random noise vector; $\mathcal{F}[n,\boldsymbol{p}]$, free energy functional
Models of dry active nematics[64,65]	$\boldsymbol{Q}(\boldsymbol{r},t) = S\left(\boldsymbol{p}\otimes\boldsymbol{p} - \frac{1}{d}\boldsymbol{I}\right)$ (8) $\partial_t \boldsymbol{Q} = -\Gamma_r \frac{\delta \mathcal{F}[n,\boldsymbol{Q}]}{\delta \boldsymbol{Q}} + \Lambda$ (9) $\partial_t n + \nabla \cdot \left(\zeta \nabla\cdot\boldsymbol{Q} + \boldsymbol{J}_{\text{passive}}\right) = 0$ (10)	S, magnitude of order parameter; $\mathcal{F}[n,\boldsymbol{Q}]$, free energy functional; Λ, white noise tensor; ζ, coefficient of active current
Scalar active model B+[69,71,72]	$\phi = (2n - n_H - n_L)/(n_H - n_L)$ (11) $\partial_t\phi + \nabla\cdot(-\lambda\nabla((\nabla\phi)^2) + \xi(\nabla^2\phi)\nabla\phi + \boldsymbol{J}_{\text{passive}} + \chi) = 0$ (12)	n_H, n_L, densities of high- and low-density coexisting phases; λ, χ, terms that break time-reversal symmetry
Fluid equations		
Incompressible Navier–Stokes equations	$\rho(\partial_t + \boldsymbol{v}\cdot\nabla)\boldsymbol{v} = -\nabla P + \nabla\cdot\boldsymbol{\sigma} + \boldsymbol{f}$ $\nabla\cdot\boldsymbol{v} = 0$ (13)	$\boldsymbol{f}$, force density; $\boldsymbol{\sigma} = \boldsymbol{\sigma}^a + \boldsymbol{\sigma}^r + \boldsymbol{\sigma}^d$, stress tensor; $\boldsymbol{\sigma}^a$, active stress; $\boldsymbol{\sigma}^r$, reversible stress due to free energy functional; $\boldsymbol{\sigma}^d = 2\eta\boldsymbol{E}$, dissipative stress
Stokes equation	$\nabla P - \nabla\cdot\boldsymbol{\sigma} - \boldsymbol{f} = 0$ (14)	$\boldsymbol{f}$, force density
Active particles in fluid		
Polar active gel models[1–3,176–181]	$D_t\boldsymbol{p} + \lambda_1(\boldsymbol{p}\cdot\nabla)\boldsymbol{p} + \ldots = \lambda E\cdot\boldsymbol{p} - \Gamma_r\frac{\delta\mathcal{F}[\boldsymbol{p}]}{\delta\boldsymbol{p}}$ (15) $\partial_t n + \nabla\cdot[(\boldsymbol{p}+\boldsymbol{v})n] = 0$ (16)	D_t, convected co-rotational time derivative; λ_1, strength of advection from polarization; λ, flow alignment coefficient; $\mathcal{F}[\boldsymbol{p}]$, free energy functional containing Frank elastic terms and terms controlling the order–disorder transition
Active nematic gel models[1–3,88,182–185]	$(\partial_t + \boldsymbol{v}\cdot\nabla)\boldsymbol{Q} = \boldsymbol{S}(E,\Omega) + \Gamma\boldsymbol{H}$ (17)	$\boldsymbol{H}$, variational derivative of the free energy; Ω, vorticity tensor; $\boldsymbol{S}$ describes competition between rotation and flow alignment
Generalized Navier–Stokes models[181,186–191]	$\boldsymbol{f} = \frac{\delta\mathcal{F}[\boldsymbol{v}]}{\delta\boldsymbol{v}}$ (18) $\boldsymbol{\sigma}^a = -\zeta\left(\boldsymbol{v}\otimes\boldsymbol{v} - \frac{v^2}{d}\boldsymbol{I}\right)$ (19) $\boldsymbol{\sigma}^d = 2\left(\Gamma_0 - \Gamma_2\nabla^2 + \Gamma_4(\nabla^2)^2\right)\boldsymbol{E}$ (20)	$\mathcal{F}[\boldsymbol{v}]$, biquadratic Landau-like free energy; ζ, activity parameter; $\boldsymbol{\sigma}^d$, generalized dissipative stress
Scalar active model H[192,193]	$\partial_t\phi + \boldsymbol{v}\cdot\nabla\phi = \Gamma_t\nabla^2\mu$ (21) $\mu = a\phi + b\phi^3 - \kappa\nabla^2\phi + \lambda(\nabla\phi)^2$ (22) $\boldsymbol{\sigma} = -\hat{\kappa}\left((\nabla\phi)\otimes(\nabla\phi) - \frac{(\nabla\phi)^2}{d}\boldsymbol{I}\right)$ (23)	ϕ, scalar order parameter; μ, chemical potential; $\lambda(\nabla\phi)^2$, active contribution to μ; $\hat{\kappa} = \kappa + \zeta \neq \kappa$

P denotes pressure, n, ρ number and mass density, $\boldsymbol{v}$ velocity, $\boldsymbol{Q}(\boldsymbol{r},t)$ nematic alignment tensor, $\boldsymbol{p}$ polarization or nematic director, $\boldsymbol{I}$ identity tensor, T temperature, Γ_t, Γ_r translational and rotational mobility, and η viscosity; $\mathbf{E} = (\nabla\boldsymbol{v} + (\nabla\boldsymbol{v})^T)/2$ is rate of strain tensor.

hydrodynamic interactions, there is no propulsion[4]. On the other hand, hydrodynamics determines the behaviour of microswimmers at walls and in channels, as well as their collective behaviour. Microscale models provide insight into the underlying physical mechanism from the level of individual microswimmers up to the emergent collective behaviours on large length scales.

Universal features

The hydrodynamics of simple Newtonian fluids is governed by the Navier–Stokes equation (see equation 13 in TABLE 1). In the limit of low Reynolds numbers,

$$\mathrm{Re} = \rho v_0 L/\eta \ll 1 \tag{3}$$

(where L is a characteristic length, v_0 a characteristic swim velocity, ρ the density of the fluid and η the dynamic viscosity), the Navier–Stokes equation reduces to the Stokes equation, for which inertial terms are negligible (equation 14 in TABLE 1). Characteristic values for microswimmers are body lengths $L \sim O(10^{-6}\mathrm{m})$ and swimming velocities $v_0 \sim O(10^{-6}\mathrm{ms}^{-1})$, hence, $\mathrm{Re} \lesssim 10^{-3}$ for water. In this limit, hydrodynamics becomes time-independent, and the dynamics is reversible. This has the important consequence that a microswimmer with a time-reversible stroke cannot propel, a phenomenon known as the scallop theorem[74].

The solution of the Stokes equation is determined by its Green's function, the Oseen tensor

$$H_{\alpha\beta}(\boldsymbol{r}) = \frac{1}{8\pi\eta r}\left[\delta_{\alpha,\beta} + r_\alpha r_\beta / r^2\right], \ (r = |\boldsymbol{r}|) \tag{4}$$

Here, δ is the Kronecker delta. The flow field obtained from H for a point force is typically denoted a Stokeslet. It is important to note that the Stokeslet does not describe an autonomous microswimmer, because the swimmer must be force-free and torque-free. Instead, a swimmer usually consists of a motor, which propels the fluid, and a cargo, which is pushed or dragged forward. Approximating these two components by point forces with opposite directions, and equal magnitude f_0, yields the dipole swimmer with the flow field of equation 24, where $P = f_0 L$ is the dipole strength (BOX 1). The sign of P distinguishes a pusher ($P > 0$, motor in the back) from a puller ($P < 0$, motor in front), with equal flow lines but opposite flow directions[4] (BOX 1). The flow field of a microswimmer is typically more complex and comprises higher-order multipoles[75,76]. However, in the far-field limit (far away from the swimmer compared with its own size), the dipole contribution (equation 24) dominates.

The dipole flow field has important consequences for the interaction of swimmers with walls[4,75,77–79] and other swimmers. Inflow generates an effective attraction; outflow generates an effective repulsion. These interactions act together with the flow-induced torque, which aligns pushers with a wall, and thus pushers are attracted to walls. Flow-induced interactions add to other interactions: an effective attraction that emerges by propulsion, slow reorientation and steric interactions (which also exist for dry active matter). Thus, flow-induced interactions are independent of whether the swimming type is pusher or puller[16,80–82]. In the case of pullers, the basic mechanism of wall interactions is arrival at the wall with the propulsion direction toward the wall, a slow reorientation determined by the rotational diffusion, during which the swimmer stays at the wall, and finally departure when the orientation points away from the wall. The hydrodynamic interactions increase the wall detention time[83].

The hydrodynamic interactions also play an important role in the nematic arrangement of elongated and rod-like microswimmers[84,85]. When the aspect ratio exceeds about 5, the nematic phase of passive rods is stable for sufficiently high volume fractions. Such an arrangement of microswimmers is sensitive to slight perturbations, for instance by a sinusoidal reorientation wave. The flow field of pushers at the nodes of this wave enhances the perturbation, and thus destabilizes the nematic phase; conversely, the flow field of pullers at nodes reduces the perturbation and stabilizes the nematic phase. This hydrodynamic instability of the nematic phase of extensile active systems lies at the heart of the intriguing dynamics of active nematics[86–89].

Hydrodynamics can also lead to high-speed and long-range communication between freely swimming cells. For example, studies of the protist *Spirostomum ambiguous* suggest that long-range vortex flows can be generated by fast cell contraction. These flows, in turn, trigger contraction of neighbouring cells and hence promote collective behaviour[90].

Swimming in viscoelastic fluids

Microorganisms often move in complex environments, which are viscoelastic rather than Newtonian. Such environments break the time-reversal symmetry of Newtonian fluids and allow for self-propulsion even for a time-symmetric internal motion, seemingly violating the scallop theorem[91]. Viscoelastic fluids are usually polymer solutions with a wide spectrum of properties, ranging from shear-thinning to viscoelastic (characterized by storage and loss moduli), and, hence, can affect the swimming behaviour of individual microswimmers[92,93] and their collective properties[94]. Theoretical studies reveal both reduced[95,96] and enhanced[97,98] swim speeds in viscoleastic media, with a transition from slow small-amplitude swimming to fast large-amplitude locomotion[97].

Viscoelastic[97,99] and shear-thinning[100] effects are typically small. However, some unexpected phenomena can appear, which are related to the complex nature of polymer solutions. Microstructured fluids generically phase-separate near surfaces, which can lead to low-viscosity fluid layers. Models show that such layers promote slip and reduce viscous friction near the surface of the swimmer, which may increase swim speeds by orders of magnitude[98]. Experiments with *Escherichia coli* in concentrated polymer solutions indicate that peculiarities of flagellated locomotion do indeed arise from the fast-rotating flagellum, leading to a lower local viscosity in its vicinity[101]. Detailed modelling and simulation of bacteria in dense polymer solutions, with explicit polymers, reach similar conclusions; in particular, polymers

Box 1 | **Microswimmer modelling across scales**

Far-field multipole expansion

The flow field $\boldsymbol{u}$ of a microswimmer is expanded in terms of multipoles (see the figure, panel **a**): force dipole (FD), source dipole (SD), force quadrupole (FQ) and so on[4,75]: $\boldsymbol{u}(\boldsymbol{r}) = \boldsymbol{u}_{FD}(\boldsymbol{r}) + \boldsymbol{u}_{SD}(\boldsymbol{r}) + \boldsymbol{u}_{FQ}(\boldsymbol{r}) + \ldots$, where $\boldsymbol{r}$ is position relative to the swimmer. The far field is determined by $\boldsymbol{u}_{FD}(\boldsymbol{r})$ (if $P \neq 0$), with

$$\boldsymbol{u}_{FD} = \frac{P\boldsymbol{r}}{8\pi\eta r^3}\left(-1 + 3\frac{(\boldsymbol{r}\cdot\hat{\boldsymbol{e}})^2}{r^2}\right) \tag{24}$$

or $\boldsymbol{u}_{SD}(\boldsymbol{r})$ (if $P = 0$)

$$\boldsymbol{u}_{SD} = \frac{\kappa_{SD}}{r^3}\left(\hat{\boldsymbol{e}} - 3\frac{\boldsymbol{z}\boldsymbol{r}}{r^2}\right) \tag{25}$$

where $\hat{\boldsymbol{e}}$ is the propulsion direction, P is the force dipole strength, and κ_{SD} accounts for the strength of the source dipole.

Coarse-grained microswimmers

Details of flow fields can be captured by the squirmer model of a microswimmer, which comprises a spheroidal solid body with a prescribed surface slip velocity. For a sphere (see the figure, panel **b**), the surface velocity is[4]

$$\boldsymbol{u}_{sq} = B_1(\sin\theta + \beta\sin\theta\cos\theta)\hat{\boldsymbol{e}}_\theta \tag{26}$$

where the first term accounts for the swim velocity v_0, the second for the active stress ($\beta < 0$ pusher, $\beta > 0$ puller). Explicitly, $B_1 = 2v_0/3$, and the multipole expansion yields $P = -6\pi\eta\, v_0 R^2\beta$ and $\kappa_{SD} = -v_0R^3/2$ for a sphere of radius R. Figure panel **c** shows a spheroidal pusher with $\beta = -3$ in the laboratory frame (left) and body-fixed frame (right).

Explicit propulsion mechanisms

We describe two such mechanisms. The first is resistive force theory[136], in which hydrodynamic interactions are included as different friction coefficients ξ parallel and perpendicular to a rod-like section of a flagellum

$$\boldsymbol{F} = \xi_{\parallel}\boldsymbol{v}_{\parallel} + \xi_{\perp}\boldsymbol{v}_{\perp} \tag{27}$$

where $\boldsymbol{F}$ is the force acting on the segment and $\boldsymbol{v}$ is its velocity. Figure panel **d** shows the time sequence of a sperm flagellum beat, from experiment (red) and resistive force theory (blue). Time increases from light to dark colours.

The other approach we discuss for modelling propulsion is to explicitly model the microswimmer and fluid. The complex flow patterns, including the near field, are resolved by microscopic models, as illustrated for a swimming *Escherichia coli* (see the figure, panel **e**). Coupling with walls leads to a particular alignment of the swimmer axis and swimming direction, as illustrated by the trajectory of the sperm head (see the figure, panel **f**).

Swimming near surfaces

The hydrodynamic interactions of a microswimmer with a wall can be described by its interaction with an image. The flow field for no-slip boundary conditions is[4,76]

$$v_w = -\frac{P}{48\pi\eta z_0^2}\left(1 - 3(\hat{\boldsymbol{e}}\cdot\hat{\boldsymbol{e}}_z)^2\right) \tag{28}$$

This flow field leads to surface trapping. The counter-rotation of cell body and flagellum bundle generates a rotlet dipole, which results in circular trajectories at surfaces with handedness depending on the slip length b, as illustrated in figure panel **g** for a slip surface ($b = \infty$)[112].

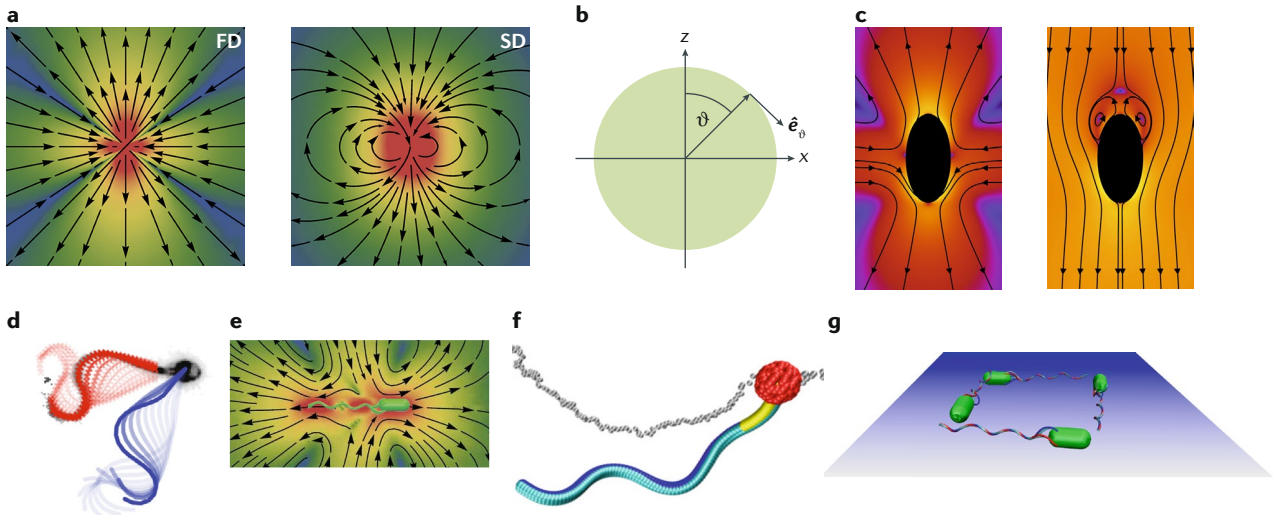

Figure: panel **a** adapted from REF.[76], Springer Nature Limited. Panel **c** adapted from REF.[128], CC-BY-3.00 (https://creativecommons.org/licenses/by/3.0/). Panel **d** adapted from REF.[137], CC-BY-4.00 (https://creativecommons.org/licenses/by/4.0/). Panel **e** adapted from REF.[112], CC-BY-3.00 (https://creativecommons.org/licenses/by/3.0/). Panel **f** adapted with permission from REF.[111], Elsevier. Panel **g** reprinted from REF.[145], CC-BY-4.00 (https://creativecommons.org/licenses/by/4.0/).

are depleted at the flagellum[102]. An increased swim speed with increasing polymer density is predicted, owing to both a non-uniform distribution of polymers in the vicinity of the bacterium — which leads to an apparent slip — and the chirality of the bacterial flagellum[102].

Mesoscale simulation techniques

To study mesocopic active-matter agents, various hydrodynamic simulation approaches have been developed. Prominent mesoscale simulation approaches are the lattice Boltzmann (LB) method[103,104], dissipative particle dynamics (DPD)[105] and the multiparticle collision dynamics (MPC) approach[106,107]. These approaches are essentially alternative ways of solving the Navier–Stokes equation and its generalizations. The LB method yields an approximate solution of the Boltzmann equation, that is, a single-particle phase-space distribution function. An advantage of LB is that thermal fluctuations can be turned on and off as desired[104]. DPD and MPC are particle-based approaches, for which the fluid is represented by point particles. DPD dynamics proceeds in an analogous way to traditional molecular dynamics

(MD) simulations, but with pairwise momentum-conserving stochastic and friction forces. By specific pairwise DPD particle interactions, compressibility of the fluid can be controlled. MPC consists of alternating streaming and collision steps, with a ballistic streaming motion and local momentum-conserving stochastic interactions (collisions), such as by rotation of relative velocities[107]. Because of the point-particle nature of the MPC particles, no fluid-induced depletion occurs, and a rather continuous representation of the fluid is obtained. Other simulation approaches implicitly take hydrodynamic interactions into account via a hydrodynamic tensor, such as the Oseen tensor (equation 4)[4], or moment expansion[75,108,109] and mobilities[110].

A microswimmer can be coupled with the fluid in various ways, depending on the nature of the microswimmer model and the desired extent of coarse-graining. Quite detailed models of, for example, sperm and *E. coli* cells yield swimming motion upon applying no-slip boundary conditions on the flagella and cell body, combined with a momentum-conserving propulsion mechanism, such as rotation of a flagellum combined with counter-rotation of the cell body. This approach applies to microswimmers in an explicit[111,112] and implicit[113–115] solvent.

Squirmers are a coarse-grained representation of microswimmers, modelled as a colloid with prescribed fluid velocity at its surface (slip velocity $\boldsymbol{v}_{sq}$)[116–119]. This representation was originally designed for ciliated microswimmers, such as *Paramecia*[119]. Nowadays, it is considered to be a generic model for a broad class of microswimmers, ranging from diffusiophoretic particles[5] to biological cells, and has been applied to study collective effects in bulk[118,120–125], at surfaces[108,120,126,127] and in narrow slits[128,129]. Typically, the slip velocity of a sphere is approximated by equation 26 in BOX 1 (REFS[117,119,128]). Extensions to prolate spheroidal microswimmers have been proposed[126,130,131]. The squirmer model has been applied with the boundary element method[118], the LB approach[120,125,127] and the MPC[129,131] representation of the fluid.

A further level of coarse-graining is to take only far-field hydrodynamics into account, and represent a microswimmer as a force dipole, in which one particle is moving in the direction of the applied force and the total momentum is conserved by imposing the opposite force on the fluid[132]. Extensions to dumbbell-type swimmers[133] or even more complex spherical[134,135] and rod-like[81,134] structures have been proposed. Such an approach allows for the study of a large number of microswimmers with minimal numerical effort. However, the near-field is inadequately accounted for[134], a deficit that is relevant for swimming behaviour near a surface, in thin slits or even the collective behaviour in dense systems.

Biological swimmers

Cell motility is essential for cellular activities such as search for food, reproduction, or escape from predators[4]. The spectrum of microswimmers is wide, including bacteria such as *E. coli*, protozoa such as dinoflagellates, algae such as *Chlamydomonas reinhardtii*, and spermatozoa. Unravelling the underlying propulsion mechanisms is essential to understand microswimmer behaviour, possibly to use them in medicine, ecology and technical applications, or to design biomimetics by transferring biological concepts to synthetic swimmers. Biological microswimmers, both prokaryotes and eukaryotes, exploit flagella for propulsion, although the structure of their flagella differs in different swimmers[4,78,136]. Bacteria typically use one or several rotating helical flagella for locomotion, whereas eukaryotes have flagella (or cilia) that beat in a wave-like fashion[137]. Explicit modelling of these microswimmers must account for three components: the cell body, the flagellum or several flagella, and the embedding fluid. Typically, such cells are considered as neutrally buoyant objects, with spherical, spheroidal or cylindrical cell body and an attached flagellum or flagella. Both parts are either considered as solid bodies[115,136,138,139] or composed of linked discrete points in a crane-like fashion for eukaryotic[111,140] or bacterial[112,113,141–144] flagella. Bacterial flagella are described by traditional polymer models or the helical worm-like chain model[4]. A bacterium is propelled by independent rotation of flagella via an applied torque. Assigning the opposite forces and torques to the cell body ensures force-free and torque-free swimming[4]. In any case, propulsion is due to frictional anisotropy of the thin flagellum[4,78,139].

Simulations emphasize the importance of hydrodynamic interactions for phenomena such as the synchronization of bacteria flagella in the bundling process for *E. coli*[141,144] or the beating of *Chlamydomonas* flagella. Moreover, they illustrate the complexity of the hydrodynamic flow field adjacent to a cell, which is important for cell–cell scattering and interaction processes[112]. Interactions of microswimmers with surfaces are fundamental in many biological processes, such as biofilm formation and egg fertilization. As pointed out above, surface hydrodynamic interactions determine the swimmer orientation[75] (BOX 1). In the far-field approximation, *E. coli* and sperm are pushers and orient preferentially parallel to a surface, whereas *Chlamydomonas* is a puller and correspondingly aligns perpendicular to surfaces. For bacteria, the rotation of the helical bundle and the counter-rotation of the cell body lead to circular trajectories with a handedness and circle radius depending on the surface slip length[145,146] — clockwise trajectories arise under no-slip[147] boundary conditions and counterclockwise trajectories for perfect-slip boundary conditions[148]. Simulations show that cells are sensitive to nanoscale changes in the surface slip length, although they themselves are significantly larger[145].

Bacterial suspensions show an intriguing chaotic state of collective motion called active turbulence[149]. Simulations of the collective behaviour of spherical squirmers exhibit cluster formation in thin films with no-slip boundary conditions (quasi-2D geometries)[129]. However, no phase separation is obtained as for ABPs[7,129]. The formation of small clusters for spherical squirmers, rather than the appearance of MIPS, is attributed to changes in the orientational dynamics by interference of the flow fields of the individual squirmers[129,150]. In contrast, spheroidal squirmers exhibit phase separation and swarming even for rather small activities[129]. Hence,

shape and hydrodynamics together govern the structure formation of active matter.

Artificial active matter

In the past decades, various artificial active agents (motors) have been synthesized, which have sizes ranging from tens of nanometres to micrometres and which exploit diverse propulsion mechanisms[5,151,152]. Common strategies are based on the slippage of fluid at the surface of the solid particle due to phoretic effects such as diffusiophoresis, involving concentration gradients; thermophoresis, involving thermal gradients; and electrophoresis by inhomogeneities in charge distributions of electrolytes[5,151–158]. Modelling of artificial active matter aims at a quantitative understanding of the underlying propulsion mechanisms and the design of strategies for practical and technological applications, such as targeted drug delivery.

In general, phoretic effects appear by molecular interactions of a solute with the solid particle (motor). Surface reactions generate inhomogeneous concentration fields of reactant and product species near the motor, leading to concentration gradients over the particle surface. These gradients cause a slippage between the fluid and the particle via diffusiophoresis and induce propulsion of the particle in the fluid. Motion is directed by controlling the surface reaction, for instance in an asymmetric reaction process on the surface of a Janus particle[5,151,159]. The theoretical description of the active process requires solving the diffusion equation for the concentration of the solute, the hydrodynamic transport problem and the solid-body equations of motion of the particle. If advection of the solute is neglected, the fluid–chemical transport problem is decoupled and the solute diffusion equation can be solved first. This solution can be exploited in the fluid problem to compute the swimming speed and the flow field[156]. The assumption that advection can be neglected applies at small Péclet numbers — defined here as the ratio of diffusion to advection timescales — as occurs at small activities, at small particle sizes or at large solute diffusion. By contrast, solute advection becomes important for large Péclet numbers and larger particles[160], and significantly impacts the solute velocity[156]. An adequate account of the interactions of the various components involved in phoresis successfully describes the salient features of artificial active particles in solution, such as swimming velocity and surface effects, as are seen for Janus particles hovering over or swimming parallel to a surface[5,161].

Response to external fields

Biological microswimmers respond to many external fields by redirecting their motion, in order to locate a target or avoid unfavourable environmental conditions. This directed motion is called taxis. Prominent examples are chemotaxis (in response to chemical gradients), phototaxis (light), gravitaxis (graviational fields), magnetotaxis (magnetic fields) and rheotaxis (flow fields). Chemotaxis is used by sperm to find the egg, phototaxis by *Chlamydomonas* algae to swim toward the light, and rheotaxis by sperm and bacteria to move upstream in flow[162–165]. Modelling and simulation have been used to understand these phenomena. For example, one mechanism of sperm chemotaxis is the response to changes in the chemoattractant concentration by adjusting the trajectory curvature with a time delay[166]. It is important to note that chemotaxis and phototaxis in biological systems often rely on internal biochemical signalling processes[167,168].

Redirection of motion in external fields also exists for artificial microswimmers. The mechanisms are usually different, and rely more on direct physical effects. Examples are gravitaxis of chiral (in 2D) L-shaped microswimmers, which can balance the hydrodynamic and gravitational torques that arise from shape asymmetry by swimming against gravity[169]; collective gravitaxis of bottom-heavy swimmers that form convective swirls in films of finite thickness[170]; and phototaxis of thermophoretic colloids, which reduce the activity of neighbouring colloids by casting a shadow on them[171].

Continuum models for active motion in fluids

To investigate phenomena occurring at large timescales and length scales, hydrodynamic theories based on conserved quantities (slow variables) and broken continuous symmetries (order parameters) have been developed, which describe a broad class of systems[172]. We discuss a few continuum models of wet active matter, that is, suspensions of active particles with momentum conservation.

Wet active liquid crystals. Of particular interest are suspensions of active rod-like or elongated objects (such as swimming organisms, cytoskeleton or tissues) embedded in a momentum-conserving solvent and generating active stresses[1–3,173–175]. The term active gel is also used in the context of the cytoskeleton and tissues, referring to their viscoelastic nature[173,174]. Slow variables are the number density $n(\boldsymbol{r},t)$ of active particles and the total momentum density $\rho\boldsymbol{v}(\boldsymbol{r},t)$ of the suspension with mass density ρ.

Polar active gels consist of particles distinguishing front from rear and are characterized by a polarization field $\boldsymbol{p}(\boldsymbol{r},t)$ corresponding to the vectorial orientation of active particles. The equations of motion for active gels are derived on the basis of symmetry[176,177] or irreversible thermodynamics[173,174,178], or by coarse-graining a microscopic theory[179,180]. The earliest phenomenological description of wet polar gels[2,176] extends the Toner–Tu model of dry active matter (equation 7), with terms that couple the orientation $\boldsymbol{p}$ to the flow, (equation 15 in TABLE 1). The fluid velocity obeys the incompressible Navier–Stokes equations (equation 13), with passive (viscous, elastic and interface) and active contributions to the stress tensor $\boldsymbol{\sigma}$; the active contributions are responsible for a spontaneous shear flow without an external stress. The assumption that every swimmer (or molecular motor) exerts an active dipolar force on the solvent (or filament network) yields, to leading order in a gradient expansion, an active stress

$$\boldsymbol{\sigma}^{\mathrm{a}} = -\zeta n(\boldsymbol{r},t)\left(\boldsymbol{p}\otimes\boldsymbol{p} - \frac{\boldsymbol{p}^2}{d}\boldsymbol{I}\right) \tag{5}$$

where d is the dimension, $\boldsymbol{I}$ the unit tensor and ζ the activity strength, that is, $\zeta > 0$ for extensile particles

(pushers) and $\zeta < 0$ for contractile particles (pullers). Note that $\boldsymbol{\sigma}^{a}$ in equation 5 has nematic symmetry, $\boldsymbol{p} \rightarrow -\boldsymbol{p}$, and active stress with purely polar symmetry arises first in terms containing gradients of $\boldsymbol{p}$ (REFS[179,181]). The concentration n of active particles evolves through the continuity equation 16.

Active gels of apolar (or head–tail symmetric) particles, called wet active nematics, are described by the nematic alignment tensor field $\boldsymbol{Q}$ introduced in equation 8 in TABLE 1, where $\boldsymbol{p}$ now denotes the nematic director. The evolution of $\boldsymbol{Q}$ in active nematics at constant concentration n is governed by the nematodynamic equation 17 (REFS[88,182–185]) accompanied by the incompressible Navier–Stokes equation (equation 13), with an active contribution $\boldsymbol{\sigma}^{a} = -\zeta \boldsymbol{Q}$ to the total stress tensor $\boldsymbol{\sigma}$; compare with equation 5. Note that dynamical equations for active nematics can be obtained from those of polar active gels by interpreting $\boldsymbol{p}$ as nematic director and dropping terms that violate the invariance of the nematic.

Generalized Navier–Stokes equations. Two-fluid models consist of equations for the fluid velocity $\boldsymbol{v}$, the concentration n and the order parameter characterizing the active constituents, such as the polarization $\boldsymbol{p}$. For dense suspensions (with constant n) it is possible to write $\boldsymbol{v}$ in terms of $\boldsymbol{p}$ or vice versa (to eliminate one of the vector fields), leading to simpler one-fluid descriptions of the system[181]. The generalized Navier–Stokes equations (GNSE) provide a class of minimal, single-vector-field models for active fluids such as dense microbial suspensions ($\boldsymbol{v}$ written in terms of $\boldsymbol{p}$, known as the bacterial flow model)[186] or sole passive solvent driven by active components ($\boldsymbol{p}$ written in terms of $\boldsymbol{v}$, known as the solvent flow model)[187].

In the bacterial flow model, $\boldsymbol{v}$ denotes the velocity of the active subcomponents, and GNSE is an extension of the Toner–Tu model, consisting of the Navier–Stokes equations plus a biquadratic Landau velocity potential $F[\boldsymbol{v}]$ (see equations 13 and 18 in TABLE 1), an active nematic stress contribution via equation 19, and higher-order terms in the Fourier expansion of the stress tensor according to equation 20 with $\Gamma_0 < 0$, $\Gamma_2 > 0$ and $\Gamma_4 = 0$ needed to account for nonlocal interactions and to reproduce local polar order observed in mesoscale turbulence[186,188,189].

The solvent dynamics in the presence of active components can be described by GNSE without a velocity potential or the active stress but with additional higher-order stresses. These higher-order terms are given by equation 20 with $\Gamma_0, \Gamma_4 > 0$ and $\Gamma_2 < 0$. They account for non-Newtonian effects[187] and originate from active stress with purely polar symmetry[181]. Solvent flow models have been used to study the rheology of active fluids[190] and active turbulence[181,191].

Active model H. Active gel models and GNSE consider the alignment interactions between active particles, either explicitly or implicitly. By contrast, the active model H (AMH) describes scalar active matter ($\boldsymbol{p} = \mathbf{Q} = 0$) and is an extension of the active model B (see equations 11 and 12 in TABLE 1), intended to account for the momentum-conserving solvent[192,193]. The dynamics of the order-parameter field $\phi(\boldsymbol{r}, t)$ obeys the diffusive equations of active model B[69,193], with an additional advective term $\boldsymbol{v} \cdot \nabla\phi$ that couples ϕ to the velocity $\boldsymbol{v}$ of the fluid, whose dynamics is governed by the Navier–Stokes equations (equation 13). The governing equations of the model are given in equations 21 and 22. The violation of the thermodynamic relation between stress $\boldsymbol{\sigma}$ and chemical potential μ leads to an active contribution to the deviatoric stress (equation 23); at interfaces, the polarization is large ($\boldsymbol{p} \sim \nabla\phi$) and equation 5 justifies equation 23. The active stress contribution is positive for extensile and negative for contractile swimmers; in the latter case, it results in an unusual arrested MIPS[192].

Cells and tissues

Living matter is active matter on all scales: on the protein scale with molecular ATP-consuming machines such as motor proteins, ATPase pumps and protein factories (the ribosome); on the cellular scale with cell shape transformation, polarization, migration and division; and on the multicellular scale with growing biofilms and tissues, tumours and developing organs.

Cytoskeletal filaments and molecular motors

The ubiquitous microscopic origin of activity in living matter is the biochemical force generation via energy-consuming polymerization and depolymerization of cytoskeleton filaments (actin and microtubules) and the collective action of molecular motors.

Force generation during polymerization of actin filaments and microtubules is based on a ratchet mechanism (BOX 2). As the filament polymerizes against a target — for instance, when pushing against the plasma membrane during the formation of filopodia or lamellipodia — thermal fluctuations of the target allow for the occasional ATP-dependent insertion of a new subunit, even when an external force opposes the motion of the target[194,195]. Asymmetric ATP-dependent polymerization and depolymerization rates at the two ends of cytoskeletal filaments also lead to their effective forward motion, a process called treadmilling[196,197] (BOX 2). Both processes are far from equilibrium and are at the heart of cell motility.

Force generation by molecular motors[198] has its origin in the massive, ATP-dependent conformational changes that occur on spatial scales from the atomic to the molecular level and timescales up to milliseconds. Elucidating the underlying molecular processes can in principle be done using all-atom MD simulations. The study of the long-timescale dynamics instead requires efficient sampling techniques and coarse-grained approaches coupled with all-atom MD simulations, termed multiscale MD simulations[199,200] (note that stability requirements demand time steps of the order of femtoseconds).

To understand the collective behaviour of whole ensembles of molecular motors and their interaction with the filament network of the cytoskeleton and the membrane, the number of degrees of freedom must be greatly reduced. Discrete kinetic and stochastic models for individual motors (BOX 2) predict the mean velocity and other observables as a function of variables including

Box 2 | **Models for cytoskeletal filaments and motors**

Treadmilling filaments

Subunits are added at the plus end of the filament with rate v_a; a protein can bind to an empty subunit with rate ω_a and detach with rate ω_d; a subunit is removed at the minus end with rate $v_d^{(e)}$ if it does not carry a protein and rate $v_d^{(o)}$ if it does (see the figure, panel **a**). The model is formulated as a master equation for the filament length and occupation of the minus end.

Force generation by polymerization of microtubules or actin filaments

This model (see the figure, panel **b**) applies the Brownian ratchet principle for polymerization-based force generation (pushing). Thermal fluctuations of the cargo allow the occasional insertion (with rate k_{on}) of a new subunit (of size δ), even when an external force F_{ext} opposes the motion of the cargo. Subunits detach with a constant rate k_{off}.

Molecular motors

Two-headed molecular motors (see the figure, panel **c**) can have hand-over-hand (left schematic) or inchworm (right schematic) stepping patterns. Mathematically, the stepping of molecular motors can be described using master equations for the position and the state of the motor.

Actomyosin as an active gel

Myosin motors pull on actin filaments, which are also linked by passive cross-linkers (see the figure, panel **d**; cross-linkers not shown). Filament polymerization and depolymerization processes have rates k_p and k_d.

Cell motility models

Schematics are given in the figure, panel **e**. In the G-actin transport model, graded protrusions of the F-actin cytoskeleton are caused by G-actin transport to the leading edge of the cell. In the vesicle transport model, the rate of protrusion at the leading edge is controlled by delivery of new cell membrane through microtubule-assisted vesicle transport. In the RAC/RHO model, the RHO GTPases RAC and RHO regulate protrusion (RAC) and contraction (RHO) within the cell. In the actomyosin contraction model, myosin binds to and contracts the actin cytoskeleton, creating cytoskeletal flows that redistribute the bound myosin.

Cell crawling on substrates

The primary physical mechanisms for substrate-based cellular motion are actin polymerization, substrate adhesion, and contraction by molecular motors (see the figure, panel **f**). A minimal phase-field model involves a phase field that describes the deformable and moveable shape of the cell, and a field for the local average orientation of the actin network. The constitutive equations account for the pushing force exerted by the actin on the cell boundary, the actin polarization dynamics (essentially localized at the cell boundary), conservation of cell area, active stresses that account for actomyosin contraction, and increased motion at the rear of the cell, which suppresses the polarization and explicitly breaks reflection symmetry[222,223].

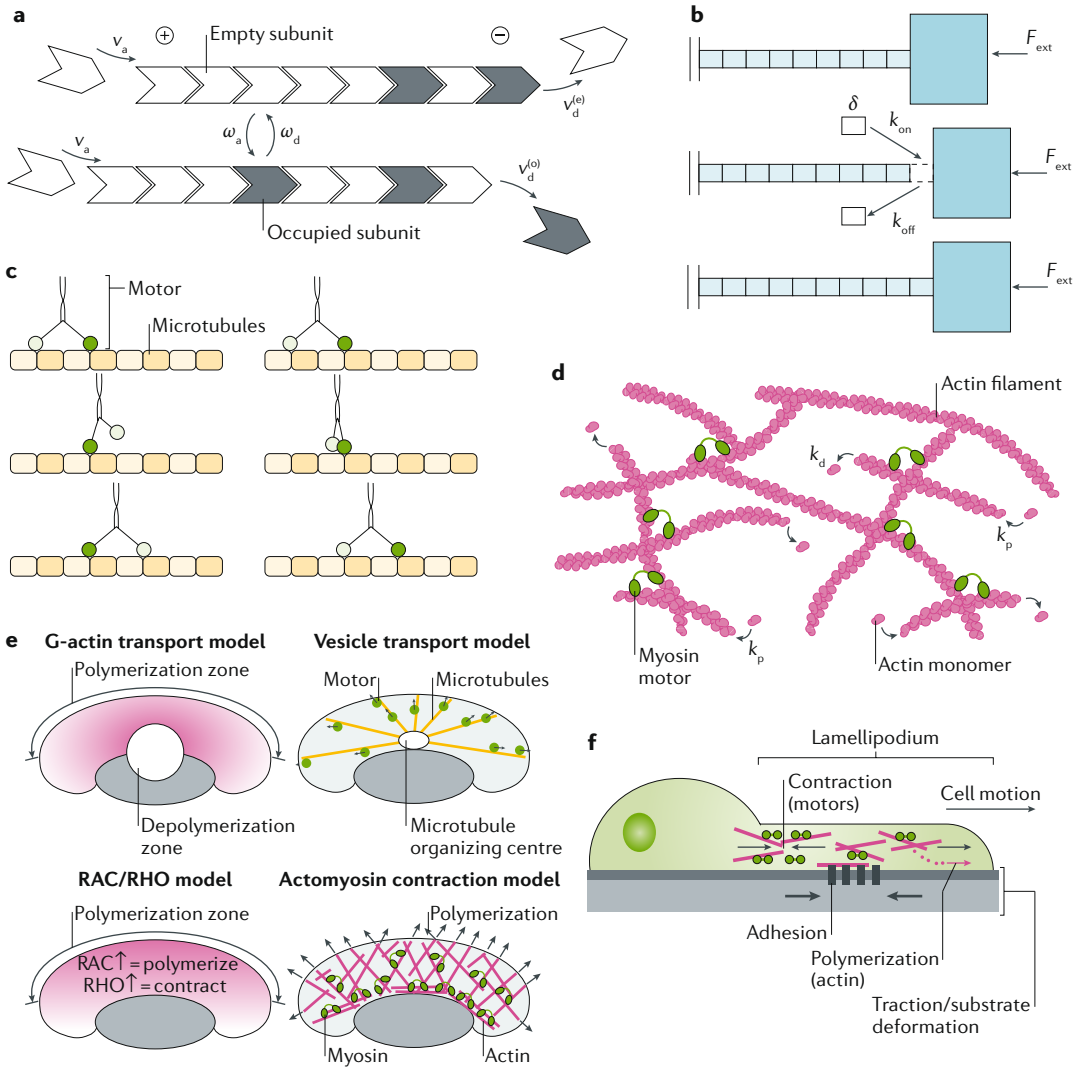

Figure: panel **a** adapted with permission from REF.[197], IOP. Panel **b** adapted with permission from REF.[195], Elsevier. Panel **c** adapted with permission from REF.[202], Elsevier. Panel **d** adapted from REF.[173], Springer Nature Limited. Panel **e** adapted with permission from REF.[221], Elsevier. Panel **f** adapted from REF.[223], Springer Nature Limited.

imposed load force and ATP concentration[201,202]. The effects of the attachment of opposing motors to one cargo are described by a tug-of-war model[203]. Many motors on a single track can lead to molecular motor traffic jams and are described by asymmetric exclusion process models[204] that are void of any mechano-chemistry.

Particle-based models for cytoskeleton filaments and networks of crosslinked filaments are based on the worm-like chain model of semiflexible polymers[205–207]. Computational studies of elastic and collective properties of semiflexible filaments are commonly based on a discretization of the filament into a finite number of segments and subsequent simulation of the Langevin dynamics. Such simulations are difficult to perform for microtubules because they are nearly incompressible in the longitudinal direction, necessitating the use of constrained Langevin dynamics (with fixed segment length), and are extremely stiff, necessitating an extremely small time step in the presence of noise — and thus noise is often neglected. Specific active aspects of microtubule dynamics comprise their length regulation[197,208] and the spindle dynamics during mitosis[209,210].

The addition of molecular motors to filament networks (for example, adding myosin to actin networks) generates forces that drive the network far from equilibrium and can markedly alter its stiffness, amplify stress or lead to network contractility. These effects were studied in an extensible worm-like chain model for semiflexible polymer in which force dipoles were introduced into the network at neighbouring crosslinks[211,212] (BOX 2). On large length and timescales, polymerizing and depolymerizing (treadmilling) actin filaments interconnected by active myosin motors and passive crosslinkers — so-called actomyosin — can be understood as an active gel for which continuum models have been developed[173,174,213,214]. From this perspective, actomyosin is an active nematic liquid described by appropriately modified Navier–Stokes equations: the central quantity is the stress tensor, which depends on the velocity gradient, the orientational field of the filaments, and an active stress generated by the motors and actin polymerization. Because cytoskeletal filaments can act as tracks to motors and in turn motors can move filaments, the active stress is coupled to the orientational field. Within this active hydrodynamics framework, cell locomotion, cellular shape changes and many experimental situations have been successfully discussed[173,174].

There are several powerful software packages for simulations of biological environments and particle-based modelling of active systems[215] (see the list and short description in Supplementary Table 1).

Cell motility models

The central molecular machinery that enables eukaryotic cells to move spontaneously is the actin cytoskeleton, which is responsible for cellular shape changes, such as the formation of thin membrane-bound protrusions. Thus, in addition to a mathematical representation of the actomyosin machinery, cell motility models must involve a representation of the cell membrane and a description of adhesion and force transmission to a substrate or a 3D environment[196,216–219]. In the paradigmatic model of cells crawling on substrates, migration is divided into discrete steps: protrusion based on actin growth and polymerization force; formation of new adhesions at the front; release and recycling of adhesions at the rear; and, finally, actin–myosin-powered contraction of the cytoplasm, resulting in forward translocation of the cell body[218] (BOX 2). In a model that relies primarily on actin treadmilling and diffusing actin nucleators, cell crawling is driven by actin polymerization waves without motors[220].

The main technical challenges for continuum modelling of cell migration are the presence of a moving boundary and the nonlinear and nonlocal coupling of cytoskeletal dynamics to a moving and deformable membrane. Three different continuum-modelling approaches for cell motility on substrates are common[217,220–224]. These are sharp-interface models, in which the interface is represented by a curve that moves with some velocity, level-set methods and diffuse-interface models. In the latter two descriptions, a phase field distinguishes the two phases (the interior and the exterior of the cell); either the position of the membrane is determined by the zero contour of the phase field, or there is a gradual variation of the different physical quantities across the interface[225]. Phase-field models have also been used for multicellular systems[226,227], for example for collective cell migration[228] (reviewed elsewhere[229]) and tissues[230,231] (BOX 3).

Alternatively, microscopic models with explicit membrane and self-propelled (pulling or pushing) filaments can be used[232,233]. These approaches incorporate fluctuations of the internal structure, persistent and random-walk-like motion and shape changes in response to external conditions.

Tissues

Tissues are aggregates of adherent cells, sometimes organized in layers (such as epithelia). Tissues can actively generate internal tension via cell proliferation and death, for instance during growth, making them viscoelasto-plastic materials[234]. Tissues also generate active stress by cellular force generation, for instance during muscle contraction. The technical challenge for a continuum formulation of volumetric growth in soft elastic tissues is the persistent change of the equilibrium configurations against which small deformations must be defined[235].

Particle-based models for tissue growth represent cells as spheres that continuously deform into dumbbells until division occurs[236,237] (BOX 3). The particles representing cells can adhere to each other, maintain volume exclusion, exert an active growth pressure on their surrounding, expand in size until they reach a size checkpoint, divide on reaching this checkpoint size, undergo apoptosis, exert random forces on neighbouring cells, regulate to their homeostatic state via cell division and apoptosis in a confined volume, and comply with force balance and momentum conservation. Both Langevin dynamics[236] and DPD[236,237] have been employed as constitutive dynamics. Simulations show that stress-induced growth inhibition is responsible for the transition from exponential to sub-exponential growth experimentally observed in tumour spheroids, and lack of nutrients

determines the size of the necrotic core but not the size of the tumour[236]. Moreover, cell division and apoptosis also lead to a fluidization of the tissue[237–239] as further analysed in a continuum theory described below.

Alternative lattice-based models for tissue growth and morphogenesis have also been used extensively. The cellular Potts model (CPM)[240–242] defines the cell shape with the help of discrete variables assigned to each site of a regular lattice (BOX 3). An energy function regulates features such as cell volume, cell surface area and cell adhesion. The CPM has been applied to development[243] and vasculogenesis[244], and also to cell migration[245] and cell shape dynamics on micropatterned surfaces[246,247]. Another lattice model is the confluent tissue vertex or Voronoi model[248–251], in which confluent monolayers are represented as a polygonal tiling of space and each polygon corresponds to a cell (BOX 3). The CPM[252] and Voronoi[253] models have been used to study the jamming transition in tissues[254].

Continuum models for tissue mechanics have a long tradition in the field of biomechanics and biomedical engineering[255]. A major challenge in continuum models for tissue growth is the coupling between growth rate and local stress, which is modelled by a dependence of the growth-rate tensor on the stress tensor[235,256,257]. A simple low-dimensional example is the mathematical

Box 3 | **Models for tissue growth**

Cellular Potts model

Individual cells are represented by a connected set of lattice unit cells (see the figure, panel **a**). In the figure, membrane sites of cell α are indicated by a darker shade, and the immediate neighbourhood of the cell is indicated by a dashed line. Elementary retraction and protrusion events directly involve a single lattice site (see the figure, panel **b**), but within a fixed range of an elementary event, the regulatory factors are increased or decreased (indicated in the figure by + and –). The cell configurations evolve stochastically by updating lattice unit cells with probabilities derived from a 'Hamiltonian' that takes into account cell contractility, cell–cell adhesion and cytoskeletal remodelling.

Vertex model for confluent monolayers

The confluent monolayer is represented by a polygonal tiling, in which each polygon corresponds to a cell. Polygons are updated in two ways (see the figure, panel **c**). One is to move the cell vertices according to deterministic equations of motion $\eta d\mathbf{x}_i(t)/dt = \boldsymbol{F}_i$, where $\mathbf{x}_i$ is the position of vertex i, $\boldsymbol{F}_i$ is the force on it (left-hand schematic). $\boldsymbol{F}_i$ comprises contributions from the cell membrane tension pointing in the directions $\hat{\boldsymbol{u}}_i^{\alpha}$ and $\hat{\boldsymbol{v}}_i^{\alpha}$, and from the cortical tension pointing in the direction $\hat{\boldsymbol{p}}_i^{\alpha}$, as indicated in the left-hand schematic. The cells also update according to graph-changing rules, such as cell neighbour exchange (upper right schematic) or division (lower right schematic). The dynamics is thus a combination of relaxation to mechanical equilibrium and changes in tissue connectivity.

Particle-based model for tissue growt

The tissue is described by an ensemble of interacting cells, in which each cell is represented by a dumbbell (see the figure, panel **d**). The dumbbells can increase the distance between spheres, representing growth, and split into two spheres, representing division (right hand schematic). These behaviours can be simulated with dissipative particle dynamics simulations. In addition, propulsion and repulsive or attractive forces can be taken into account by conservative interactions.

Multicellular phase-field models

The shape of cell i is defined by a phase field $\phi_i(x)$ that ranges from 0 to 1. Dynamics are defined by a set of equations analogous to the phase-field description of single-cell migration. The repulsion of two cells i and j involves the product $\phi_i(x)\phi_j(x)$, which is non-zero only where the two phase fields overlap (see the figure, panel **e**).

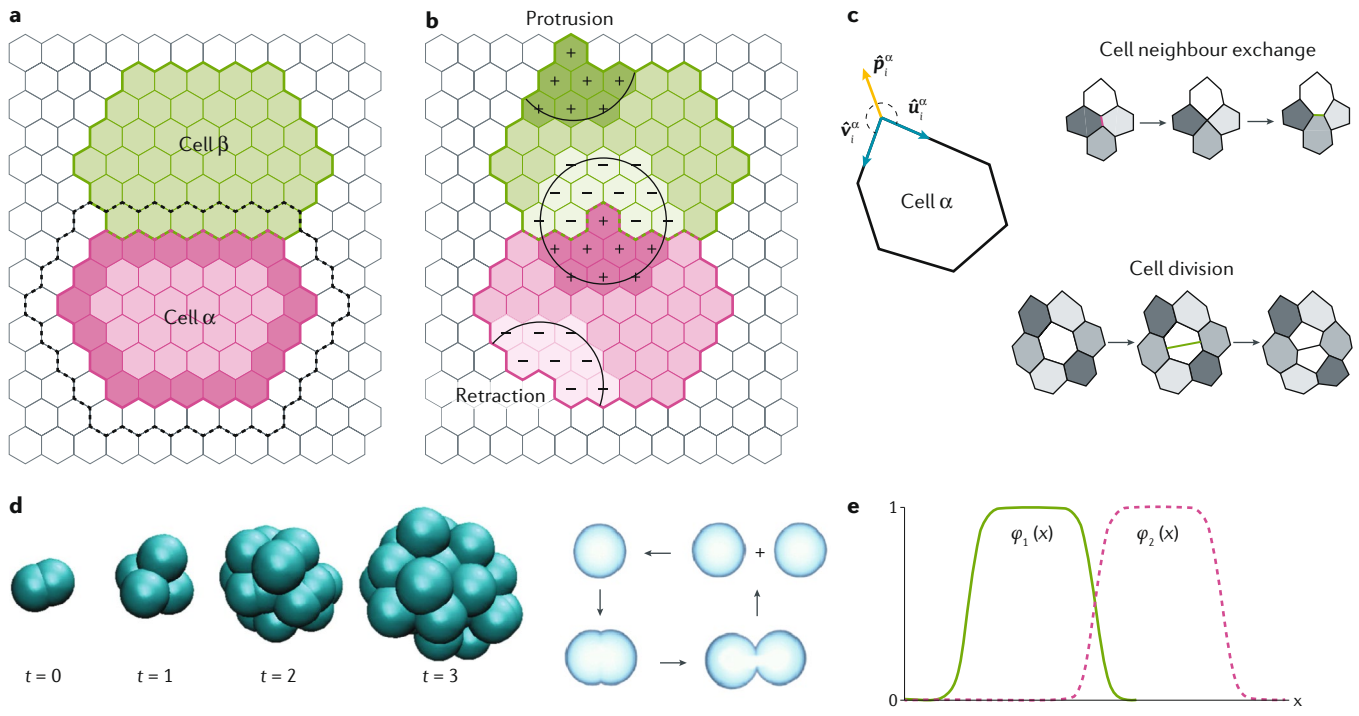

Figure: panels **a** and **b** adapted with permission from REF.[247], APS. Panel **c** adapted with permission from REF.[249], Elsevier. Panel **d** adapted with permission from REF.[63], PNAS, and REF.[236], IOP. Panel **e** adapted with permission from REF.[229], IOP.

model of non-uniform growth in a monolayer[258], which incorporates a mechanical feedback mechanism via an explicit dependence of the local tissue growth rate on the degree of local compression (or stretching). In another approach, 3D tissues were considered as elastic media, and it was shown that the coupling of cell division and cell death to the local stresses effectively leads to viscoelastic behaviour with a relaxation time set by the rate of cell division[63].

Finally, various continuum models for tumour growth are based on the theory of mixtures[259] (reviewed elsewhere[260]). Because tissue growth in a living organism requires nutrition supply and oxygen, a blood vessel network should be included. To this end, hybrid models describe the tumour mass with a continuum model and the dynamically changing vascularization with a discrete pipe network[261,262]. Simulations show that the incorporation of a blood vessel network leads to a characteristic compartmentalization of the tumour into several regions that differ in vessel density, vessel diameter and level of necrosis.

Animal groups

Many animals, including swarms of insects, fish schools, bird flocks, herds of game and human crowds, engage in collective migration. The models of dry active matter (FIG. 2), in particular the Vicsek model and its extensions[44], capture prototypical aspects of the collective behaviour of such animal groups. Despite sharing some universal features, the observed motion patterns differ substantially among animal groups. These differences arise from differences in the nature of interactions between individuals and require adaptation of basic models. Important characteristics include social behaviour mediated by chemical, acoustic or optical signals. Chemical signalling comprises non-reciprocal attractive–repulsive interactions, which lead to specific actions such as pursuit–escape behaviour[263–265]. Particular attention has been paid to modelling vision-based interactions, for which the emerging motion patterns depend on the field of view[266–268].

The mechanisms underlying the collective behaviour of animal groups can be studied through several strategies. In a phenomenological top-down approach, (physical) interactions are deduced from observations[268,269]. Alternatively, in a bottom-up approach, the effect of complex information processing strategies of individual agents, such as delayed signal processing, is studied[270–272]. Collective behaviour can even emerge from a purely probabilistic model that considers intrinsic motivation and maximization of future options via processing of sensed information, without any a priori

Box 4 | **Computational methods for simulating active matter**

Molecular dynamics (MD)
Standard approach to solve Newton's equations of motion. For active matter, energy input and a thermostat are required to drive the system out of equilibrium and to allow for a stationary state for long times.

Brownian dynamics (BD) and Langevin dynamics (LD)
Particle dynamics is described by (overdamped) Newtonian equations of motion with noise and active forces.

Kinetic Monte Carlo (KMC)
A series of Monte Carlo steps is performed for the configurational variables. The acceptance probability can be obtained from importance sampling with the energy difference between original and attempted new state, for example. Usually applied to lattice tissue-growth models such as the cellular Potts model.

Lattice Boltzmann (LB)
Mesoscale hydrodynamics approach, based on propagating velocity distribution functions on lattices. The standard version does not include thermal fluctuations and is therefore well-suited for larger microswimmers.

Dissipative particle dynamics (DPD)
Particle-based mesoscale hydrodynamics approach, which generalizes MD by including noise and pairwise friction forces. Multiphase flows are readily incorporated as direct conservative interactions between different particle species. Active particles are coupled to the fluid by non-conservative forces.

Multiparticle collision dynamics (MPC)
Particle-based mesoscale hydrodynamics approach that uses an ensemble of point particles for the fluid with multiparticle collisions in a regular lattice of collision boxes. Naturally includes thermal fluctuations. Avoids depletion interactions between active solutes and is therefore well-suited for active systems with small characteristic length scales.

Boundary integral method (BIM)
Hydrodynamic interactions are integrated out by the use of Green's functions of the Stokes equation, in favour of forces between boundary elements of walls and embedded active particles. Active systems are modelled by non-conservative boundary forces.

Direct numerical simulation (DNS)
Solution of the Navier–Stokes equations on a lattice by finite-element or finite-volume methods, in which all spatial scales are resolved in the computational mesh. Coupling to active particles is achieved through boundary conditions.

Coloured noise
The effect of active fluids on embedded passive particles is different from thermal fluctuations, owing to finite persistence times, which can be captured by memory kernels or active noise.

Cellular Potts model
Lattice-based model for the dynamics of cell populations and tissues (in 2D and 3D). Useful when the intercellular interactions are determined by the shape and size of individual cells and the contact area between neighbouring cells. Individual cells are represented by multiple connected lattice sites, which are updated stochastically via KMC.

Vertex model
Discrete model in continuum 2D space for the dynamics of confluent cell monolayers. Useful when the intercellular interactions are determined by the shape and size of individual cells and the contact area between neighbouring cells. The confluent monolayer is represented as a polygonal tiling in which each polygon corresponds to a cell. Polygons are updated by moving their vertices according to deterministic equations of motion and a set of graph-changing rules.

Phase-field model
Continuum model to describe the dynamics of individual cells and cell populations. Useful to describe actin-driven cell migration and shape transformations. Individual cells are represented by a phase field that interacts with other fields such as the local actin polarization. Tissues are described by multiple phase fields, each corresponding to a cell. The interaction between neighbouring cells is determined by the overlap of their phase fields, and the spatiotemporal evolution is defined by partial differential equations.

specification of social forces or individual interaction rules[271,273].

Living active agents travelling together have developed efficient decision-making mechanisms during evolution for behaviours such as searching, foraging and escaping. For instance, quorum sensing — the ability of individuals to coordinate their activities according to the local population density — facilitates information transfer[267,274,275]. Although such cooperative interactions are powerful tools to reach collective decisions[276], in some cases only a few individuals possess the required knowledge about the migration route, location of food sources or other goal[277]. Accordingly, numerical models have been applied to the mechanisms of effective leadership in biological systems and the impact of the density of informed individuals and their communications on information transfer in animal groups[278–280]. A realistic description of collective human motion is crucial to prevent crowd disasters[281–283].

Outlook

Many powerful computational models for active matter, particle-based or field-theoretical, have been developed in the recent years (see a list of computational methods for active matter in BOX 4). These models have revealed much about the non-equilibrium behaviour of active systems. Yet many challenges remain.

The statistical-physics description of active systems needs to be extended in several directions, including the incorporation of an activity-dependent noise to account for the stochastic nature of active forces, and the generalization of field-theoretical models to systems far from equilibrium. Current field theories are based on a linear expansion of fluxes in terms of forces and can therefore in principle describe only systems close to equilibrium; however, biological systems are typically far from equilibrium, and as yet there is no comprehensive continuum theory for such systems.

So far, the investigation of the collective behaviour of self-propelled particles has been limited to relatively simple systems. However, we expect that many surprises will be found when different ingredients of systems are combined. These ingredients include interactions, such as shape and hydrodynamics; complex environments, such as viscoelastic fluids and intricate confining geometries; external fields, such as gravity and turbulent flows; mixtures of active and passive particles; and information exchange by vision-like interactions.

Many models for cell motility have been used in studies of migration on 2D substrates. However, many cells in living organisms move in 3D environments, such as the extracellular matrix (ECM), and there is a lack of continuum models for motility in 3D. Initial studies have focused on rigidity sensing and subsequent polarization of the cell toward stiffer ECM[284]. Furthermore, to migrate in 3D environments, cells can move in ways other than adhesion-based lamellipodial propulsion, in particular via blebbing motility, which is based on the formation of blebs at the leading edge (blebs emerge when the plasma membrane of a cell delaminates locally from its actin cortex, leading to pressure-driven protrusions, followed by membrane re-attachment)[285]. The first modelling studies of blebbing-induced migration in 2D[286] and of amoeboid migration in 3D[287] still crucially depend on protrusions adhering to a substrate.

Finally, signalling is a very important aspect of cell motility, tissue growth, the development of bacterial colonies and the collective motion of animal herds, but has been neglected in most computational models for active matter. One challenge is to model the interplay of biochemistry and mechanics on a single-cell level[288–290]. Another challenge is modelling the reaction of flocks, schools and herds to external factors such as food, smell or light. Quantitative models for tissue growth, morphogenesis, biofilm formation, wound healing, or cancer growth and metastasis need to include biochemical signalling coupled to mechanical stress. Similarly, realistic models for human groups, car or pedestrian traffic need to take into account heterogeneous behaviour and varying reactions of individuals to external cues; doing so also asks for the investigation of a putative leader role.

An overarching challenge for the whole field is the distinction between the generic and specific properties and behaviour of an active-matter system. In other words, the question is what properties are universal and shared by a large class of systems, and when specific mechanisms of propulsion or interactions dominate the behaviour.

Published online 10 March 2020

1. Marchetti, M. C. et al. Hydrodynamics of soft active matter. *Rev. Mod. Phys.* **85**, 1143–1189 (2013). **Comprehensive overview of the hydrodynamic theories of active matter**.
2. Ramaswamy, S. The mechanics and statistics of active matter. *Annu. Rev. Condens. Matter Phys.* **1**, 323–345 (2010).
3. Toner, J., Tu, Y. & Ramaswamy, S. Hydrodynamics and phases of flocks. *Ann. Phys.* **318**, 170–244 (2005).
4. Elgeti, J., Winkler, R. G. & Gompper, G. Physics of microswimmers—single particle motion and collective behavior: a review. *Rep. Prog. Phys.* **78**, 056601 (2015). **Review of theories, simulations and experiments on microswimmers**.
5. Bechinger, C. et al. Active particles in complex and crowded environments. *Rev. Mod. Phys.* **88**, 045006 (2016). **Guided tour of artificial self-propelling microparticles and nanoparticles, and their application to the study of nonequilibrium phenomena**.
6. Solon, A. P. et al. Pressure is not a state function for generic active fluids. *Nat. Phys.* **11**, 673–678 (2015).
7. Bialké, J., Speck, T. & Löwen, H. Crystallization in a dense suspension of self-propelled particles. *Phys. Rev. Lett.* **108**, 168301 (2012).
8. Redner, G. S., Hagan, M. F. & Baskaran, A. Structure and dynamics of a phase-separating active colloidal fluid. *Phys. Rev. Lett.* **110**, 055701 (2013).
9. Cates, M. E. & Tailleur, J. Motility-induced phase separation. *Annu. Rev. Condens. Matter Phys.* **6**, 219–244 (2015). **Review of theoretical descriptions of motility-induced phase separation in active matter**.
10. Wysocki, A., Winkler, R. G. & Gompper, G. Cooperative motion of active Brownian spheres in three-dimensional dense suspensions. *Europhys. Lett.* **105**, 48004 (2014).
11. Stenhammar, J., Marenduzzo, D., Allen, R. J. & Cates, M. E. Phase behaviour of active Brownian particles: the role of dimensionality. *Soft Matter* **10**, 1489–1499 (2014).
12. Wysocki, A., Winkler, R. G. & Gompper, G. Propagating interfaces in mixtures of active and passive Brownian particles. *New J. Phys.* **18**, 123030 (2016).
13. Stenhammar, J., Wittkowski, R., Marenduzzo, D. & Cates, M. E. Activity-induced phase separation and self-assembly in mixtures of active and passive particles. *Phys. Rev. Lett.* **114**, 018301 (2015).
14. Digregorio, P. et al. Full phase diagram of active Brownian disks: from melting to motility-induced phase separation. *Phys. Rev. Lett.* **121**, 098003 (2018).
15. Fily, Y., Henkes, S. & Marchetti, M. C. Freezing and phase separation of self-propelled disks. *Soft Matter* **10**, 2132–2140 (2014).
16. Elgeti, J. & Gompper, G. Wall accumulation of self-propelled spheres. *EPL* **101**, 48003 (2013).
17. Fily, Y., Baskaran, A. & Hagan, M. Dynamics of self-propelled particles under strong confinement. *Soft Matter* **10**, 5609–5617 (2014).
18. Das, S., Gompper, G. & Winkler, R. G. Local stress and pressure in an inhomogeneous system of spherical active Brownian particles. *Sci. Rep.* **9**, 6608 (2019).

19. Wysocki, A. & Rieger, H. Capillary action in scalar active matter. *Phys. Rev. Lett.* **124**, 048001 (2019).
20. Takatori, S. C., Yan, W. & Brady, J. F. Swim pressure: stress generation in active matter. *Phys. Rev. Lett.* **113**, 028103 (2014).
21. Winkler, R. G., Wysocki, A. & Gompper, G. Virial pressure in systems of active Brownian particles. *Soft Matter* **11**, 6680–6691 (2015).
22. Fily, Y., Kafri, Y., Solon, A. P., Tailleur, J. & Turner, A. Mechanical pressure and momentum conservation in dry active matter. *J. Phys. A* **51**, 044003 (2018).
23. Wysocki, A., Elgeti, J. & Gompper, G. Giant adsorption of microswimmers: duality of shape asymmetry and wall curvature. *Phys. Rev. E* **91**, 050302(R) (2015).
24. Romanczuk, P., Bär, M., Ebeling, W., Lindner, B. & Schimansky-Geier, L. Active Brownian particles. *Eur. Phys. J. Spec. Top.* **202**, 1–162 (2012).
25. Nguyen, N. H. P., Klotsa, D., Engel, M. & Glotzer, S. C. Emergent collective phenomena in a mixture of hard shapes through active rotation. *Phys. Rev. Lett.* **112**, 075701 (2014).
26. Löwen, H. Chirality in microswimmer motion: from circle swimmers to active turbulence. *Eur. Phys. J. Spec. Top.* **225**, 2319–2331 (2016).
27. Peruani, F. Active Brownian rods. *Eur. Phys. J. Spec. Top.* **225**, 2301–2317 (2016).
28. ten Hagen, B. et al. Can the self-propulsion of anisotropic microswimmers be described by using forces and torques? *J. Phys. Condens. Matter* **27**, 194110 (2015).
29. Kaiser, A., Babel, S., ten Hagen, B., von Ferber, C. & Löwen, H. How does a flexible chain of active particles swell? *J. Chem. Phys.* **142**, 124905 (2015).
30. Eisenstecken, T., Gompper, G. & Winkler, R. G. Conformational properties of active semiflexible polymers. *Polymers* **8**, 304 (2016).
31. Eisenstecken, T., Gompper, G. & Winkler, R. G. Internal dynamics of semiflexible polymers with active noise. *J. Chem. Phys.* **146**, 154903 (2017).
32. Kourbane-Houssene, M., Erignoux, C., Bodineau, T. & Tailleur, J. Exact hydrodynamic description of active lattice gases. *Phys. Rev. Lett.* **120**, 268003 (2018).
33. Klamser, J. U., Kapfer, S. C. & Krauth, W. Thermodynamic phases in two-dimensional active matter. *Nat. Commun.* **9**, 5045 (2018).
34. Sadjadi, Z., Shaebani, M. R., Rieger, H. & Santen, L. Persistent-random-walk approach to anomalous transport of self-propelled particles. *Phys. Rev. E* **91**, 062715 (2015).
35. Shaebani, M. R., Sadjadi, Z., Sokolov, I. M., Rieger, H. & Santen, L. Anomalous diffusion of self-propelled particles in directed random environments. *Phys. Rev. E* **90**, 030701 (2014).
36. Levis, D. & Berthier, L. Clustering and heterogeneous dynamics in a kinetic Monte Carlo model of self-propelled hard disks. *Phys. Rev. E* **89**, 062301 (2014).
37. Najafi, J. et al. Flagellar number governs bacterial spreading and transport efficiency. *Sci. Adv.* **4**, eaar6425 (2018).
38. Hafner, A. E., Santen, L., Rieger, H. & Shaebani, M. R. Run-and-pause dynamics of cytoskeletal motor proteins. *Sci. Rep.* **6**, 37162 (2016).
39. Vicsek, T. & Zafeiris, A. Collective motion. *Phys. Rep.* **517**, 71–140 (2012).
Review of collective motion of active agents, from macromolecules through metallic rods and robots to groups of animals and people.
40. Vicsek, T., Czirók, A., Ben-Jacob, E., Cohen, I. & Shochet, O. Novel type of phase transition in a system of self-driven particles. *Phys. Rev. Lett.* **75**, 1226–1229 (1995).
41. Solon, A. P., Chaté, H. & Tailleur, J. From phase to microphase separation in flocking models: the essential role of nonequilibrium fluctuations. *Phys. Rev. Lett.* **114**, 068101 (2015).
42. Solon, A. P. & Tailleur, J. Revisiting the flocking transition using active spins. *Phys. Rev. Lett.* **111**, 078101 (2013).
43. Ginelli, F., Peruani, F., Bär, M. & Chaté, H. Large-scale collective properties of self-propelled rods. *Phys. Rev. Lett.* **104**, 184502 (2010).
44. Chaté, H., Ginelli, F., Grégoire, G., Peruani, F. & Raynaud, F. Modeling collective motion: variations on the vicsek model. *Eur. Phys. J. B* **64**, 451–456 (2008).
45. Strömbom, D. Collective motion from local attraction. *J. Theor. Biol.* **283**, 145–151 (2011).
46. Aldana, M., Dossetti, V., Huepe, C., Kenkre, V. M. & Larralde, H. Phase transitions in systems of self-propelled agents and related network models. *Phys. Rev. Lett.* **98**, 095702 (2007).
47. Aldana, M., Larralde, H. & Vazquez, B. On the emergence of collective order in swarming systems: a recent debate. *Int. J. Mod. Phys. B* **23**, 3661–3685 (2009).
48. Peruani, F. & Aranson, I. S. Cold active motion: how time-independent disorder affects the motion of self-propelled agents. *Phys. Rev. Lett.* **120**, 238101 (2018).
49. Grossman, D., Aranson, I. S. & Jacob, E. B. Emergence of agent swarm migration and vortex formation through inelastic collisions. *New J. Phys.* **10**, 023036 (2008).
50. Nagy, M., Daruka, I. & Vicsek, T. New aspects of the continuous phase transition in the scalar noise model (snm) of collective motion. *Physica A* **373**, 445–454 (2007).
51. Peruani, F., Klauss, T., Deutsch, A. & Voss-Boehme, A. Traffic jams, gliders, and bands in the quest for collective motion of self-propelled particles. *Phys. Rev. Lett.* **106**, 128101 (2011).
52. Ginelli, F. & Chaté, H. Relevance of metric-free interactions in flocking phenomena. *Phys. Rev. Lett.* **105**, 168103 (2010).
53. Gregoire, G., Chaté, H. & Tu, Y. Moving and staying together without a leader. *Physica D* **181**, 157–170 (2003).
54. Szabó, P., Nagy, M. & Vicsek, T. Transitions in a self-propelled-particles model with coupling of accelerations. *Phys. Rev. E* **79**, 021908 (2009).
55. Chaté, H., Ginelli, F. & Montagne, R. Simple model for active nematics: quasi-long-range order and giant fluctuations. *Phys. Rev. Lett.* **96**, 180602 (2006).
56. Mahault, B. et al. Self-propelled particles with velocity reversals and ferromagnetic alignment: active matter class with second-order transition to quasi-long-range polar order. *Phys. Rev. Lett.* **120**, 258002 (2018).
57. Szabó, B. et al. Phase transition in the collective migration of tissue cells: experiment and model. *Phys. Rev. E* **74**, 061908 (2006).
58. Peruani, F., Deutsch, A. & Bär, M. Nonequilibrium clustering of self-propelled rods. *Phys. Rev. E* **74**, 030904 (2006).
59. Toner, J. & Tu, Y. Long-range order in a two-dimensional dynamical XY model: how birds fly together. *Phys. Rev. Lett.* **75**, 4326–4329 (1995).
60. Toner, J. & Tu, Y. Flocks, herds, and schools: a quantitative theory of flocking. *Phys. Rev. E* **58**, 4828–4858 (1998).
61. Bertin, E., Droz, M. & Grégoire, G. Boltzmann and hydrodynamic description for self-propelled particles. *Phys. Rev. E* **74**, 022101 (2006).
62. Ihle, T. Kinetic theory of flocking: derivation of hydrodynamic equations. *Phys. Rev. E* **83**, 030901 (2011).
63. Ranft, J. et al. Fluidization of tissues by cell division and apoptosis. *Proc. Natl Acad. Sci. USA* **107**, 20863–20868 (2010).
64. Narayan, V., Ramaswamy, S. & Menon, N. Long-lived giant number fluctuations in a swarming granular nematic. *Science* **317**, 105–108 (2007).
65. Ramaswamy, S., Simha, R. A. & Toner, J. Active nematics on a substrate: giant number fluctuations and long-time tails. *EPL* **62**, 196–202 (2003).
66. Hemingway, E. J. et al. Active viscoelastic matter: from bacterial drag reduction to turbulent solids. *Phys. Rev. Lett.* **114**, 098302 (2015).
67. Schwarz, U. S. & Safran, S. A. Physics of adherent cells. *Rev. Mod. Phys.* **85**, 1327–1381 (2013).
68. Hohenberg, P. C. & Halperin, B. I. Theory of dynamic critical phenomena. *Rev. Mod. Phys.* **49**, 435–479 (1977).
69. Wittkowski, R. et al. Scalar ϕ^4 field theory for active-particle phase separation. *Nat. Commun.* **5**, 4351 (2014).
70. Tjhung, E., Nardini, C. & Cates, M. E. Cluster phases and bubbly phase separation in active fluids: reversal of the ostwald process. *Phys. Rev. X* **8**, 031080 (2018).
71. Stenhammar, J., Tiribocchi, A., Allen, R. J., Marenduzzo, D. & Cates, M. E. Continuum theory of phase separation kinetics for active Brownian particles. *Phys. Rev. Lett.* **111**, 145702 (2013).
72. Cates, M. E. & Tailleur, J. When are active Brownian particles and run-and-tumble particles equivalent? Consequences for motility-induced phase separation. *EPL* **101**, 20010 (2013).
73. Tailleur, J. & Cates, M. E. Statistical mechanics of interacting run-and-tumble bacteria. *Phys. Rev. Lett.* **100**, 218103 (2008).
74. Purcell, E. M. Life at low Reynolds number. *Am. J. Phys.* **45**, 3–11 (1977).
75. Spagnolie, S. E. & Lauga, E. Hydrodynamics of self-propulsion near a boundary: predictions and accuracy of far-field approximations. *J. Fluid Mech.* **700**, 105–147 (2012).
76. Winkler, R. G. & Gompper, G. in *Handbook of Materials Modeling: Methods: Theory and Modeling* (eds Andreoni, W. & Yip, S.) 1–20 (Springer, 2018).
77. Berke, A. P., Turner, L., Berg, H. C. & Lauga, E. Hydrodynamic attraction of swimming microorganisms by surfaces. *Phys. Rev. Lett.* **101**, 038102 (2008).
78. Lauga, E. & Powers, T. R. The hydrodynamics of swimming microorganisms. *Rep. Prog. Phys.* **72**, 096601 (2009).
79. Elgeti, J. & Gompper, G. Microswimmers near surfaces. *Eur. Phys. J. Spec. Top.* **225**, 2333–2352 (2016).
80. Li, G. & Tang, J. X. Accumulation of microswimmers near a surface mediated by collision and rotational Brownian motion. *Phys. Rev. Lett.* **103**, 078101 (2009).
81. Elgeti, J. & Gompper, G. Self-propelled rods near surfaces. *EPL* **85**, 38002 (2009).
82. Elgeti, J. & Gompper, G. Run-and-tumble dynamics of self-propelled particles in confinement. *EPL* **109**, 58003 (2015).
83. Schaar, K., Zöttl, A. & Stark, H. Detention times of microswimmers close to surfaces: influence of hydrodynamic interactions and noise. *Phys. Rev. Lett.* **115**, 038101 (2015).
84. Saintillan, D. & Shelley, M. J. Orientational order and instabilities in suspensions of self-locomoting rods. *Phys. Rev. Lett.* **99**, 058102 (2007).
85. Saintillan, D. & Shelley, M. J. Instabilities and pattern formation in active particle suspensions: kinetic theory and continuum simulations. *Phys. Rev. Lett.* **100**, 178103 (2008).
86. Sanchez, T., Chen, D. T. N., DeCamp, S. J., Heymann, M. & Dogic, Z. Spontaneous motion in hierarchically assembled active matter. *Nature* **491**, 431–434 (2012).
87. Thampi, S. P., Golestanian, R. & Yeomans, J. M. Velocity correlations in an active nematic. *Phys. Rev. Lett.* **111**, 118101 (2013).
88. Giomi, L., Bowick, M. J., Ma, X. & Marchetti, M. C. Defect annihilation and proliferation in active nematics. *Phys. Rev. Lett.* **110**, 228101 (2013).
89. Keber, F. C. et al. Topology and dynamics of active nematic vesicles. *Science* **345**, 1135–1139 (2014).
90. Mathijssen, A. J. T. M., Culver, J., Bhamla, M. S. & Prakash, M. Collective intercellular communication through ultra-fast hydrodynamic trigger waves. *Nature* **571**, 560–564 (2019).
91. Qiu, T. et al. Swimming by reciprocal motion at low Reynolds number. *Nat. Commun.* **5**, 5119 (2014).
92. Qin, B., Gopinath, A., Yang, J., Gollub, J. P. & Arratia, P. E. Flagellar kinematics and swimming of algal cells in viscoelastic fluids. *Sci. Rep.* **5**, 9190 (2015).
93. Patteson, A. E., Gopinath, A., Goulian, M. & Arratia, P. E. Running and tumbling with *E. coli* in polymeric solutions. *Sci. Rep.* **5**, 15761 (2015).
94. Li, G. & Ardekani, A. M. Collective motion of microorganisms in a viscoelastic fluid. *Phys. Rev. Lett.* **117**, 118001 (2016).
95. Lauga, E. Propulsion in a viscoelastic fluid. *Phys. Fluids* **19**, 083104 (2007).
96. Fu, H. C., Wolgemuth, C. W. & Powers, T. R. Swimming speeds of filaments in nonlinearly viscoelastic fluids. *Phys. Fluids* **21**, 033102 (2009).
97. Spagnolie, S. E., Liu, B. & Powers, T. R. Locomotion of helical bodies in viscoelastic fluids: enhanced swimming at large helical amplitudes. *Phys. Rev. Lett.* **111**, 068101 (2013).
98. Man, Y. & Lauga, E. Phase-separation models for swimming enhancement in complex fluids. *Phys. Rev. E* **92**, 023004 (2015).
99. Liu, B., Powers, T. R. & Breuer, K. S. Force-free swimming of a model helical flagellum in viscoelastic fluids. *Proc. Natl Acad. Sci. USA* **108**, 19516–19520 (2011).
100. Gagnon, D. A., Keim, N. C. & Arratia, P. E. Undulatory swimming in shear-thinning fluids: experiments with *Caenorhabditis elegans*. *J. Fluid Mech.* **758**, R3 (2014).
101. Martinez, V. A. et al. Flagellated bacterial motility in polymer solutions. *Proc. Natl Acad. Sci. USA* **111**, 17771–17776 (2014).
102. Zöttl, A. & Yeomans, J. M. Enhanced bacterial swimming speeds in macromolecular polymer solutions. *Nat. Phys.* **15**, 554–558 (2019).
103. McNamara, G. R. & Zanetti, G. Use of the Boltzmann equation to simulate lattice-gas automata. *Phys. Rev. Lett.* **61**, 2332–2335 (1988).
104. Dünweg, B. & Ladd, A. J. C. Lattice Boltzmann simulations of soft matter systems. *Adv. Polym. Sci.* **221**, 89–166 (2009).

105. Español, P. & Warren, P. Statistical mechanics of dissipative particle dynamics. *EPL* **30**, 191–196 (1995).
106. Kapral, R. *Advances in Chemical Physics* (Wiley, 2008).
107. Gompper, G., Ihle, T., Kroll, D. M. & Winkler, R. G. Multi-particle collision dynamics: a particle-based mesoscale simulation approach to the hydrodynamics of complex fluids. *Adv. Polym. Sci.* **221**, 1–87 (2009).
108. Ishikawa, T. & Pedley, T. J. Coherent structures in monolayers of swimming particles. *Phys. Rev. Lett.* **100**, 088103 (2008).
109. Mathijssen, A. J. T. M., Doostmohammadi, A., Yeomans, J. M. & Shendruk, T. N. Hydrodynamics of micro-swimmers in films. *J. Fluid Mech.* **806**, 35–70 (2016).
110. Singh, R., Ghose, S. & Adhikari, R. Many-body microhydrodynamics of colloidal particles with active boundary layers. *J. Stat. Mech. Theor. Exp.* **2015**, P06017 (2015).
111. Elgeti, J., Kaupp, U. B. & Gompper, G. Hydrodynamics of sperm cells near surfaces. *Biophys. J.* **99**, 1018–1026 (2010).
112. Hu, J., Yang, M., Gompper, G. & Winkler, R. G. Modelling the mechanics and hydrodynamics of swimming *E. coli*. *Soft Matter* **11**, 7867–7876 (2015).
113. Watari, N. & Larson, R. G. The hydrodynamics of a run-and-tumble bacterium propelled by polymorphic helical flagella. *Biophys. J.* **98**, 12–17 (2010).
114. Shum, H.,Gaffney, E. A. & Smith D. J. Modelling bacterial behaviour close to a no-slip plane boundary: the influence of bacterial geometry. *Proc. R. Soc. A* **466**, 1725–1748 (2010).
115. Pimponi, D., Chinappi, M., Gualtieri, P. & Casciola, C. M. Hydrodynamics of flagellated microswimmers near free-slip interfaces. *J. Fluid Mech.* **789**, 514–533 (2016).
116. Lighthill, M. J. On the squirming motion of nearly spherical deformable bodies through liquids at very small Reynolds numbers. *Comm. Pure Appl. Math.* **5**, 109–118 (1952).
117. Blake, J. R. A spherical envelope approach to ciliary propulsion. *J. Fluid Mech.* **46**, 199–208 (1971).
118. Ishikawa, T., Simmonds, M. P. & Pedley, T. J. Hydrodynamic interaction of two swimming model micro-organisms. *J. Fluid Mech.* **568**, 119–160 (2006).
119. Pedley, T. J. Spherical squirmers: models for swimming micro-organisms. *IMA J. Appl. Math.* **81**, 488–521 (2016).
120. Llopis, I. & Pagonabarraga, I. Hydrodynamic interactions in squirmer motion: swimming with a neighbour and close to a wall. *J. Nonnewton. Fluid Mech.* **165**, 946–952 (2010).
121. Götze, I. O. & Gompper, G. Mesoscale simulations of hydrodynamic squirmer interactions. *Phys. Rev. E* **82**, 041921 (2010).
122. Evans, A. A., Ishikawa, T., Yamaguchi, T. & Lauga, E. Orientational order in concentrated suspensions of spherical microswimmers. *Phys. Fluids* **23**, 111702 (2011).
123. Alarcon, F. & Pagonabarraga, I. Spontaneous aggregation and global polar ordering in squirmer suspensions. *J. Mol. Liq.* **185**, 56–61 (2013).
124. Molina, J. J., Nakayama, Y. & Yamamoto, R. Hydrodynamic interactions of self-propelled swimmers. *Soft Matter* **9**, 4923–4936 (2013).
125. Yoshinaga, N. & Liverpool, T. B. Hydrodynamic interactions in dense active suspensions: from polar order to dynamical clusters. *Phys. Rev. E* **96**, 020603 (2017).
126. Ishimoto, K. & Gaffney, E. A. Squirmer dynamics near a boundary. *Phys. Rev. E* **88**, 062702 (2013).
127. Lintuvuori, J. S., Brown, A. T., Stratford, K. & Marenduzzo, D. Hydrodynamic oscillations and variable swimming speed in squirmers close to repulsive walls. *Soft Matter* **12**, 7959–7968 (2016).
128. Theers, M., Westphal, E., Gompper, G. & Winkler, R. G. Modeling a spheroidal microswimmer and cooperative swimming in a narrow slit. *Soft Matter* **12**, 7372–7385 (2016).
129. Theers, M., Westphal, E., Qi, K., Winkler, R. G. & Gompper, G. Clustering of microswimmers: interplay of shape and hydrodynamics. *Soft Matter* **14**, 8590–8603 (2018).
130. Keller, S. R. & Wu, T. Y. A porous prolate-spheroidal model for ciliated micro-organisms. *J. Fluid Mech.* **80**, 259–278 (1977).
131. Theers, M., Westphal, E., Gompper, G. & Winkler, R. G. From local to hydrodynamic friction in Brownian motion: a multiparticle collision dynamics simulation study. *Phys. Rev. E* **93**, 032604 (2016).
132. Nash, R. W., Adhikari, R., Tailleur, J. & Cates, M. E. Run-and-tumble particles with hydrodynamics: sedimentation, trapping, and upstream swimming. *Phys. Rev. Lett.* **104**, 258101 (2010).
133. Hernandez-Ortiz, J. P., Stoltz, C. G. & Graham, M. D. Transport and collective dynamics in suspensions of confined swimming particles. *Phys. Rev. Lett.* **95**, 204501 (2005).
134. de Graaf, J. et al. Lattice Boltzmann hydrodynamics of anisotropic active matter. *J. Chem. Phys.* **144**, 134106 (2016).
135. Menzel, A. M., Saha, A., Hoell, C. & Löwen, H. Dynamical density functional theory for microswimmers. *J. Chem. Phys.* **144**, 024115 (2016).
136. Lighthill, J. Flagellar hydrodynamics. *SIAM Rev.* **18**, 161–230 (1976).
137. Saggiorato, G. et al. Human sperm steer with second harmonics of the flagellar beat. *Nat. Commun.* **8**, 1415 (2017).
138. Shum, H. & Gaffney, E. A. Hydrodynamic analysis of flagellated bacteria swimming near one and between two no-slip plane boundaries. *Phys. Rev. E* **91**, 033012 (2015).
139. Lauga, E. Bacterial hydrodynamics. *Annu. Rev. Fluid Mech.* **48**, 105–130 (2016).
Comprehensive review of the hydrodynamics of bacteria.
140. Rode, S., Elgeti, J. & Gompper, G. Sperm motility in modulated microchannels. *New J. Phys.* **21**, 013016 (2019).
141. Reigh, S. Y., Winkler, R. G. & Gompper, G. Synchronization and bundling of anchored bacterial flagella. *Soft Matter* **8**, 4363–4372 (2012).
142. Reichert, M. & Stark, H. Synchronization of rotating helices by hydrodynamic interactions. *Eur. Phys. J. E* **17**, 493–500 (2005).
143. Vogel, R. & Stark, H. Motor-driven bacterial flagella and buckling instabilities. *Eur. Phys. J. E* **35**, 15 (2012).
144. Janssen, P. J. A. & Graham, M. D. Coexistence of tight and loose bundled states in a model of bacterial flagellar dynamics. *Phys. Rev. E* **84**, 011910 (2011).
145. Hu, J., Wysocki, A., Winkler, R. G. & Gompper, G. Physical sensing of surface properties by microswimmers - directing bacterial motion via wall slip. *Sci. Rep.* **5**, 9586 (2015).
146. Lemelle, L., Palierne, J.-F., Chatre, E., Vaillant, C. & Place, C. Curvature reversal of the circular motion of swimming bacteria probes for slip at solid/liquid interfaces. *Soft Matter* **9**, 9759–9762 (2013).
147. Lauga, E., DiLuzio, W. R., Whitesides, G. M. & Stone, H. A. Swimming in circles: motion of bacteria near solid boundaries. *Biophys. J.* **90**, 400–412 (2006).
148. Di Leonardo, R., Dell Arciprete, D., Angelani, L. & Iebba, V. Swimming with an image. *Phys. Rev. Lett.* **106**, 038101 (2011).
149. Dombrowski, C., Cisneros, L., Chatkaew, S., Goldstein, R. E. & Kessler, J. O. Self-concentration and large-scale coherence in bacterial dynamics. *Phys. Rev. Lett.* **93**, 098103 (2004).
150. Matas-Navarro, R., Golestanian, R., Liverpool, T. B. & Fielding, S. M. Hydrodynamic suppression of phase separation in active suspensions. *Phys. Rev. E* **90**, 032304 (2014).
151. Gaspard, P. & Kapral, R. Thermodynamics and statistical mechanics of chemically powered synthetic nanomotors. *Adv. Phys. X* **4**, 1602480 (2019).
152. Bayati, P., Popescu, M. N., Uspal, W. E., Dietrich, S. & Najafi, A. Dynamics near planar walls for various model self-phoretic particles. *Soft Matter* **15**, 5644–5672 (2019).
153. Rückner, G. & Kapral, R. Chemically powered nanodimers. *Phys. Rev. Lett.* **98**, 150603 (2007).
154. Yang, M. & Ripoll, M. Simulations of thermophoretic nanoswimmers. *Phys. Rev. E* **84**, 061401 (2011).
155. Saha, S., Golestanian, R. & Ramaswamy, S. Clusters, asters, and collective oscillations in chemotactic colloids. *Phys. Rev. E* **89**, 062316 (2014).
156. Michelin, S. & Lauga, E. Phoretic self-propulsion at finite Péclet numbers. *J. Fluid Mech.* **747**, 572 (2014).
157. Liebchen, B., Marenduzzo, D., Pagonabarraga, I. & Cates, M. E. Clustering and pattern formation in chemorepulsive active colloids. *Phys. Rev. Lett.* **115**, 258301 (2015).
158. Stark, H. Artificial chemotaxis of self-phoretic active colloids: collective behavior. *Acc. Chem. Res.* **51**, 2681–2688 (2018).
159. Moran, J. L. & Posner, J. D. Phoretic self-propulsion. *Annu. Rev. Fluid Mech.* **49**, 511–540 (2017).
160. Howse, J. R. et al. Self-motile colloidal particles: from directed propulsion to random walk. *Phys. Rev. Lett.* **99**, 048102 (2007).
161. Uspal, W. E., Popescu, M. N., Dietrich, S. & Tasinkevych, M. Self-propulsion of a catalytically active particle near a planar wall: from reflection to sliding and hovering. *Soft Matter* **11**, 434 (2015).
162. Ishimoto, K. & Gaffney, E. A. Fluid flow and sperm guidance: a simulation study of hydrodynamic sperm rheotaxis. *J. Roy. Soc. Interface* **12**, 20150172 (2015).
163. Koh, J. B. Y., Shen, X. & Marcos. Theoretical modeling in microscale locomotion. *Microfluid. Nanofluid.* **20**, 98 (2016).
164. Uspal, W. E., Popescu, M. N., Dietrich, S. & Tasinkevych, M. Rheotaxis of spherical active particles near a planar wall. *Soft Matter* **11**, 6613–6632 (2015).
165. Mathijssen, A. et al. Oscillatory surface rheotaxis of swimming *E. coli* bacteria. *Nat. Commun.* **20**, 3434 (2019).
166. Friedrich, B. M. & Jülicher, F. Chemotaxis of sperm cells. *Proc. Natl Acad. Sci. USA* **104**, 13256 (2007).
167. Tu, Y. Quantitative modeling of bacterial chemotaxis: signal amplification and accurate adaptation. *Annu. Rev. Biophys.* **42**, 337–359 (2013).
168. Camley, B. A., Zimmermann, J., Levine, H. & Rappel, W.-J. Emergent collective chemotaxis without single-cell gradient sensing. *Phys. Rev. Lett.* **116**, 098101 (2016).
169. ten Hagen, B. et al. Gravitaxis of asymmetric self-propelled colloidal particles. *Nat. Commun.* **5**, 4829 (2014).
170. Kuhr, J.-T., Blaschke, J., Rühle, F. & Stark, H. Collective sedimentation of squirmers under gravity. *Soft Matter* **13**, 7548–7555 (2017).
171. Cohen, J. A. & Golestanian, R. Emergent cometlike swarming of optically driven thermally active colloids. *Phys. Rev. Lett.* **112**, 068302 (2014).
172. Martin, P. C., Parodi, O. & Pershan, P. S. Unified hydrodynamic theory for crystals, liquid crystals, and normal fluids. *Phys. Rev. A* **6**, 2401–2420 (1972).
173. Prost, J., Jülicher, F. & Joanny, J.-F. Active gel phys. *Nat. Phys.* **11**, 111–117 (2015).
Introduction to active-gel models for actomyosin.
174. Jülicher, F., Grill, S. W. & Salbreux, G. Hydrodynamic theory of active matter. *Rep. Prog. Phys.* **81**, 076601 (2018).
175. Carenza, L. N., Gonnella, G., Lamura, A., Negro, G. & Tiribocchi, A. Lattice Boltzmann methods and active fluids. *Eur. Phys. J. E* **42**, 81 (2019).
176. AditiSimha, R. & Ramaswamy, S. Hydrodynamic fluctuations and instabilities in ordered suspensions of self-propelled particles. *Phys. Rev. Lett.* **89**, 058101 (2002).
177. Hatwalne, Y., Ramaswamy, S., Rao, M. & Simha, R. A. Rheology of active-particle suspensions. *Phys. Rev. Lett.* **92**, 118101 (2004).
178. Kruse, K., Joanny, J. F., Jülicher, F., Prost, J. & Sekimoto, K. Asters, vortices, and rotating spirals in active gels of polar filaments. *Phys. Rev. Lett.* **92**, 078101 (2004).
179. Giomi, L., Marchetti, M. C. & Liverpool, T. B. Complex spontaneous flows and concentration banding in active polar films. *Phys. Rev. Lett.* **101**, 198101 (2008).
180. Baskaran, A. & Marchetti, M. C. Statistical mechanics and hydrodynamics of bacterial suspensions. *Proc. Natl Acad. Sci. USA* **106**, 15567–15572 (2009).
181. Linkmann, M., Marchetti, M. C., Boffetta, G. & Eckhardt, B. Condensate formation and multiscale dynamics in two-dimensional active suspensions. Preprint at *arXiv* https://arxiv.org/abs/1905.06267 (2019).
182. Marenduzzo, D., Orlandini, E., Cates, M. E. & Yeomans, J. M. Steady-state hydrodynamic instabilities of active liquid crystals: hybrid lattice Boltzmann simulations. *Phys. Rev. E* **76**, 031921 (2007).
183. Marenduzzo, D., Orlandini, E. & Yeomans, J. M. Hydrodynamics and rheology of active liquid crystals: a numerical investigation. *Phys. Rev. Lett.* **98**, 118102 (2007).
184. Giomi, L., Mahadevan, L., Chakraborty, B. & Hagan, M. F. Excitable patterns in active nematics. *Phys. Rev. Lett.* **106**, 218101 (2011).
185. Doostmohammadi, A., Ignes-Mullol, J., Yeomans, J. M. & Sagues, F. Active nematics. *Nat. Commun.* **9**, 3246 (2018).
186. Dunkel, J., Heidenreich, S., Bär, M. & Goldstein, R. E. Minimal continuum theories of structure formation in dense active fluids. *New J. Phys.* **15**, 045016 (2013).

187. Slomka, J. & Dunkel, J. Generalized Navier-Stokes equations for active suspensions. *Eur. Phys. J. Spec. Top.* **224**, 1349–1358 (2015).
188. Dunkel, J. et al. Fluid dynamics of bacterial turbulence. *Phys. Rev. Lett.* **110**, 228102 (2013).
189. Wensink, H. H. et al. Meso-scale turbulence in living fluids. *Proc. Natl Acad. Sci. USA* **109**, 14308–14313 (2012).
190. Slomka, J. & Dunkel, J. Geometry-dependent viscosity reduction in sheared active fluids. *Phys. Rev. Fluids* **2**, 043102 (2017).
191. Slomka, J. & Dunkel, J. Spontaneous mirror-symmetry breaking induces inverse energy cascade in 3D active fluids. *Proc. Natl Acad. Sci. USA* **114**, 2119–2124 (2017).
192. Tiribocchi, A., Wittkowski, R., Marenduzzo, D. & Cates, M. E. Active model H: scalar active matter in a momentum-conserving fluid. *Phys. Rev. Lett.* **115**, 188302 (2015).
193. Cates, M. E. Active field theories. Preprint at *arXiv* https://arxiv.org/abs/1904.01330 (2019).
194. Mogilner, A. & Oster, G. Cell motility driven by actin polymerization. *Biophys. J.* **71**, 3030–3045 (1996).
195. Dogterom, M., Kerssemakers, J. W., Romet-Lemonne, G. & Janson, M. E. Force generation by dynamic microtubules. *Curr. Opin. Cell Biol.* **17**, 67–74 (2005).
196. Mogilner, A. Mathematics of cell motility: have we got its number? *J. Math. Biol.* **58**, 105 (2008).
197. Erlenkämper, C. & Kruse, K. Uncorrelated changes of subunit stability can generate length-dependent disassembly of treadmilling filaments. *Phys. Biol.* **6**, 046016 (2009).
198. Howard, J. & Kruse, K. *Mechanics of Motor Proteins and the Cytoskeleton* (Sinauer Associates, 2001).
199. Nielsen, S. O., Bulo, R. E., Moore, P. B. & Ensing, B. Recent progress in adaptive multiscale molecular dynamics simulations of soft matter. *Phys. Chem. Chem. Phys.* **12**, 12401–12414 (2010).
200. Ekimoto, T. & Ikeguchi, M. Multiscale molecular dynamics simulations of rotary motor proteins. *Biophys. Rev.* **10**, 605–615 (2018).
201. Kolomeisky, A. B. & Fisher, M. E. Molecular motors: a theorist's perspective. *Annu. Rev. Phys. Chem.* **58**, 675–695 (2007).
202. Chowdhury, D. Stochastic mechano-chemical kinetics of molecular motors: a multidisciplinary enterprise from a physicist's perspective. *Phys. Rep.* **529**, 1–197 (2013).
Physicist's view on molecular motors.
203. Klumpp, S. & Lipowsky, R. Cooperative cargo transport by several molecular motors. *Proc. Natl Acad. Sci. USA* **102**, 17284–17289 (2005).
204. Appert-Rolland, C., Ebbinghaus, M. & Santen, L. Intracellular transport driven by cytoskeletal motors: general mechanisms and defects. *Phys. Rep.* **593**, 1–59 (2015).
205. Bausch, A. R. & Kroy, K. A bottom-up approach to cell mechanics. *Nat. Phys.* **2**, 231–238 (2006).
206. Huber, F. et al. Emergent complexity of the cytoskeleton: from single filaments to tissue. *Adv. Phys.* **62**, 1–112 (2013).
207. Broedersz, C. P. & MacKintosh, F. C. Modeling semiflexible polymer networks. *Rev. Mod. Phys.* **86**, 995–1036 (2014).
208. Mohapatra, L., Goode, B. L., Jelenkovic, P., Phillips, R. & Kondev, J. Design principles of length control of cytoskeletal structures. *Annu. Rev. Biophys.* **45**, 85–116 (2016).
209. Mogilner, A. & Craig, E. Towards a quantitative understanding of mitotic spindle assembly and mechanics. *J. Cell Sci.* **123**, 3435–3445 (2010).
210. Pavin, N. & Tolić, I. M. Self-organization and forces in the mitotic spindle. *Annu. Rev. Biophys.* **45**, 279–298 (2016).
211. Broedersz, C. P. & MacKintosh, F. C. Molecular motors stiffen non-affine semiflexible polymer networks. *Soft Matter* **7**, 3186–3191 (2011).
212. Ronceray, P., Broedersz, C. P. & Lenz, M. Fiber networks amplify active stress. *Proc. Natl Acad. Sci. USA* **113**, 2827–2832 (2016).
213. Jülicher, F., Kruse, K., Prost, J. & Joanny, J.-F. Active behavior of the cytoskeleton. *Phys. Rep.* **449**, 3–28 (2007).
214. Joanny, J. F. & Prost, J. Active gels as a description of the actin–myosin cytoskeleton. *HFSP J.* **3**, 94–104 (2009).
215. Nedelec, F. & Foethke, D. Collective langevin dynamics of flexible cytoskeletal fibers. *New J. Phys.* **9**, 427–427 (2007).
216. Jilkine, A. & Edelstein-Keshet, L. A comparison of mathematical models for polarization of single eukaryotic cells in response to guided cues. *PLoS Comput. Biol.* **7**, e1001121 (2011).
217. Holmes, W. R. & Edelstein-Keshet, L. A comparison of computational models for eukaryotic cell shape and motility. *PLoS Comput. Biol.* **8**, e1002793 (2012).
218. Danuser, G., Allard, J. & Mogilner, A. Mathematical modeling of eukaryotic cell migration: insights beyond experiments. *Annu. Rev. Cell Dev. Biol.* **29**, 501–528 (2013).
Comprehensive overview of mathematical modelling of cell migration.
219. te Boekhorst, V., Preziosi, L. & Friedl, P. Plasticity of cell migration in vivo and in silico. *Annu. Rev. Cell Dev. Biol.* **32**, 491–526 (2016).
220. Doubrovinski, K. & Kruse, K. Cell motility resulting from spontaneous polymerization waves. *Phys. Rev. Lett.* **107**, 258103 (2011).
221. Wolgemuth, C. W., Stajic, J. & Mogilner, A. Redundant mechanisms for stable cell locomotion revealed by minimal models. *Biophys. J.* **101**, 545–553 (2011).
222. Ziebert, F., Swaminathan, S. & Aranson, I. S. Model for self-polarization and motility of keratocyte fragments. *J. R. Soc. Interface* **9**, 1084–1092 (2012).
223. Ziebert, F. & Aranson, I. S. Computational approaches to substrate-based cell motility. *NPJ Comput. Mater.* **2**, 16019 (2016).
224. Linsmeier, I. et al. Disordered actomyosin networks are sufficient to produce cooperative and telescopic contractility. *Nat. Commun.* **7**, 12615 (2016).
225. Singer-Loginova, I. & Singer, H. M. The phase field technique for modeling multiphase materials. *Rep. Prog. Phys.* **71**, 106501 (2008).
226. Nonomura, M. Study on multicellular systems using a phase field model. *PLoS One* **7**, 1–9 (2012).
227. Camley, B. A. et al. Polarity mechanisms such as contact inhibition of locomotion regulate persistent rotational motion of mammalian cells on micropatterns. *Proc. Natl Acad. Sci. USA* **111**, 14770–14775 (2014).
228. Najem, S. & Grant, M. Phase-field model for collective cell migration. *Phys. Rev. E* **93**, 052405 (2016).
229. Camley, B. A. & Rappel, W.-J. Physical models of collective cell motility: from cell to tissue. *J. Phys. D* **50**, 113002 (2017).
Overview of physical models describing collective motion of cells and tissues.
230. Mueller, R., Yeomans, J. M. & Doostmohammadi, A. Emergence of active nematic behavior in monolayers of isotropic cells. *Phys. Rev. Lett.* **122**, 048004 (2019).
231. Wenzel, D., Praetorius, S. & Voigt, A. Topological and geometrical quantities in active cellular structures. *J. Chem. Phys.* **150**, 164108 (2019).
232. Abaurrea-Velasco, C., Ghahnaviyeh, S. D., Pishkenari, H. N., Auth, T. & Gompper, G. Complex self-propelled rings: a minimal model for cell motility. *Soft Matter* **13**, 5865–5876 (2017).
233. Abaurrea-Velasco, C., Auth, T. & Gompper, G. Vesicles with internal active filaments: self-organized propulsion controls shape, motility, and dynamical response. *New J. Phys.* https://doi.org/10.1088/1367-2630/ab5c70 (2019).
234. Preziosi, L., Ambrosi, D. & Verdier, C. An elasto-visco-plastic model of cell aggregates. *J. Theor. Biol.* **262**, 35–47 (2010).
235. Rodriguez, E. K., Hoger, A. & McCulloch, A. D. Stress-dependent finite growth in soft elastic tissues. *J. Biomech.* **27**, 455–467 (1994).
236. Drasdo, D. & Höhme, S. A single-cell-based model of tumor growth in vitro: monolayers and spheroids. *Phys. Biol.* **2**, 133–147 (2005).
237. Basan, M., Prost, J., Joanny, J.-F. & Elgeti, J. Dissipative particle dynamics simulations for biological tissues: rheology and competition. *Phys. Biol.* **8**, 026014 (2011).
238. Malmi-Kakkada, A. N., Li, X., Samanta, H. S., Sinha, S. & Thirumalai, D. Cell growth rate dictates the onset of glass to fluidlike transition and long time superdiffusion in an evolving cell colony. *Phys. Rev. X* **8**, 021025 (2018).
239. Matoz-Fernandez, D. A., Martens, K., Sknepnek, R., Barrat, J. L. & Henkes, S. Cell division and death inhibit glassy behaviour of confluent tissues. *Soft Matter* **13**, 3205–3212 (2017).
240. Graner, F. & Glazier, J. A. Simulation of biological cell sorting using a two-dimensional extended potts model. *Phys. Rev. Lett.* **69**, 2013–2016 (1992).
241. Glazier, J. A. & Graner, F. Simulation of the differential adhesion driven rearrangement of biological cells. *Phys. Rev. E* **47**, 2128–2154 (1993).
242. Chen, N., Glazier, J. A., Izaguirre, J. A. & Alber, M. S. A parallel implementation of the cellular Potts model for simulation of cell-based morphogenesis. *Comput. Phys. Commun.* **176**, 670–681 (2007).
243. Maree, A. F. M. & Hogeweg, P. How amoeboids self-organize into a fruiting body: multicellular coordination in dictyostelium discoideum. *Proc. Natl Acad. Sci. USA* **98**, 3879–3883 (2001).
244. Merks, R. M. H., Perryn, E. D., Shirinifard, A. & Glazier, J. A. Contact-inhibited chemotaxis in de novo and sprouting blood-vessel growth. *PLoS Comp. Biol.* **4**, e1000163 (2008).
245. Maree, A. F. M., Jilkine, A., Dawes, A., Grieneisen, V. A. & Edelstein-Keshet, L. Polarization and movement of keratocytes: a multiscale modelling approach. *Bull. Math. Biol.* **68**, 1169–1211 (2006).
246. Albert, P. J. & Schwarz, U. S. Dynamics of cell shape and forces on micropatterned substrates predicted by a cellular potts model. *Biophys. J.* **106**, 2340–2352 (2014).
247. Segerer, F. J., Thüroff, F., PieraAlberola, A., Frey, E. & Rädler, J. O. Emergence and persistence of collective cell migration on small circular micropatterns. *Phys. Rev. Lett.* **114**, 228102 (2015).
248. Hufnagel, L., Teleman, A. A., Rouault, H., Cohen, S. M. & Shraiman, B. I. On the mechanism of wing size determination in fly development. *Proc. Natl Acad. Sci. USA* **104**, 3835–3840 (2007).
249. Fletcher, A. G., Osterfield, M., Baker, R. E. & Shvartsman, S. Y. Vertex models of epithelial morphogenesis. *Biophys. J.* **106**, 2291–2304 (2014).
250. Sussman, D. M., Schwarz, J. M., Marchetti, M. C. & Manning, M. L. Soft yet sharp interfaces in a vertex model of confluent tissue. *Phys. Rev. Lett.* **120**, 058001 (2018).
251. Barton, D. L., Henkes, S., Weijer, C. J. & Sknepnek, R. Active vertex model for cell-resolution description of epithelial tissue mechanics. *PLoS Comput. Biol.* **13**, e1005569 (2017).
252. Chiang, M. & Marenduzzo, D. Glass transitions in the cellular Potts model. *Europhys. Lett.* **116**, 28009 (2016).
253. Bi, D., Yang, X., Marchetti, M. C. & Manning, M. L. Motility-driven glass and jamming transitions in biological tissues. *Phys. Rev. X* **6**, 021011 (2016).
254. Oswald, L., Grosser, S., Smith, D. M. & Käs, J. A. Jamming transitions in cancer. *J. Phys. D* **50**, 483001 (2017).
Review of tissue dynamics and liquid-like versus solid-like behaviour.
255. Fung, Y.-C. *Biomechanics: Mechanical Properties of Living Tissues* 2nd edn (Springer, 2010).
256. Dunlop, J. W. C., Fischer, F. D., Gamsjäger, E. & Fratzl, P. A theoretical model for tissue growth in confined geometries. *J. Mech. Phys. Solids* **58**, 1073–1087 (2010).
257. Ambrosi, D., Preziosi, L. & Vitale, G. The interplay between stress and growth in solid tumors. *Mech. Res. Commun.* **42**, 87–91 (2012).
258. Shraiman, B. I. Mechanical feedback as a possible regulator of tissue growth. *Proc. Natl Acad. Sci. USA* **102**, 3318–3323 (2005).
259. Byrne, H. & Preziosi, L. Modelling solid tumour growth using the theory of mixtures. *Math. Med. Biol.* **20**, 341–366 (2003).
260. Tracqui, P. Biophysical models of tumour growth. *Rep. Prog. Phys.* **72**, 056701 (2009).
261. Rieger, H. & Welter, M. Integrative models of vascular remodeling during tumor growth. *WIREs Syst. Biol. Med.* **7**, 113–129 (2015).
262. Fredrich, T., Rieger, H., Chignola, R. & Milotti, E. Fine-grained simulations of the microenvironment of vascularized tumours. *Sci. Rep.* **9**, 11698 (2019).
263. Romanczuk, P., Couzin, I. D. & Schimansky-Geier, L. Collective motion due to individual escape and pursuit response. *Phys. Rev. Lett.* **102**, 010602 (2009).
264. Simpson, S. J., Sword, G. A., Lorch, P. D. & Couzin, I. D. Cannibal crickets on a forced march for protein and salt. *Proc. Natl Acad. Sci. USA* **103**, 4152–4156 (2006).
265. Agudo-Canalejo, J. & Golestanian, R. Active phase separation in mixtures of chemically interacting particles. *Phys. Rev. Lett.* **123**, 018101 (2019).
266. Pearce, D. J. G., Miller, A. M., Rowlands, G. & Turner, M. S. Role of projection in the control of bird flocks. *Proc. Natl Acad. Sci. USA* **111**, 10422–10426 (2014).
267. Lavergne, F. A., Wendehenne, H., Bäuerle, T. & Bechinger, C. Group formation and cohesion of active particles with visual perception-dependent motility. *Science* **364**, 70–74 (2019).
268. Ballerini, M. et al. Interaction ruling animal collective behavior depends on topological rather than metric distance: evidence from a field study. *Proc. Natl Acad. Sci. USA* **105**, 1232–1237 (2008).
269. Bajec, I. L. & Heppner, F. H. Organized flight in birds. *Animal Behav.* **78**, 777–789 (2009).

270. Mijalkov, M., McDaniel, A., Wehr, J. & Volpe, G. Engineering sensorial delay to control phototaxis and emergent collective behaviors. *Phys. Rev. X* **6**, 011008 (2016).
271. Charlesworth, H. J. & Turner, M. S. Intrinsically motivated collective motion. *Proc. Natl Acad. Sci. USA* **116**, 15362–15367 (2019).
272. Khadka, U., Holubec, V., Yang, H. & Cichos, F. Active particles bound by information flows. *Nat. Commun.* **9**, 3864 (2018).
273. Mann, R. P. & Garnett, R. The entropic basis of collective behaviour. *J. R. Soc. Interface* **12**, 20150037 (2015).
274. Ward, A. J. W., Sumpter, D. J. T., Couzin, I. D., Hart, P. J. B. & Krause, J. Quorum decision-making facilitates information transfer in fish shoals. *Proc. Natl Acad. Sci. USA* **105**, 6948–6953 (2008).
275. Abaurrea Velasco, C., Abkenar, M., Gompper, G. & Auth, T. Collective behavior of self-propelled rods with quorum sensing. *Phys. Rev. E* **98**, 022605 (2018).
276. Castellano, C., Fortunato, S. & Loreto, V. Statistical physics of social dynamics. *Rev. Mod. Phys.* **81**, 591–646 (2009).
277. King, A. J., Douglas, C. M., Huchard, E., Isaac, N. J. & Cowlishaw, G. Dominance and affiliation mediate despotism in a social primate. *Curr. Biol.* **18**, 1833–1838 (2008).
278. Couzin, I. D., Krause, J., Franks, N. R. & Levin, S. A. Effective leadership and decision-making in animal groups on the move. *Nature* **433**, 513–516 (2005).
279. Freeman, R. & Biro, D. Modelling group navigation: dominance and democracy in homing pigeons. *J. Navigat.* **62**, 33–40 (2009).
280. Bäuerle, T., Fischer, A., Speck, T. & Bechinger, C. Self-organization of active particles by quorum sensing rules. *Nat. Commun.* **9**, 3232 (2018).
281. Moussaïd, M., Helbing, D. & Theraulaz, G. How simple rules determine pedestrian behavior and crowd disasters. *Proc. Natl Acad. Sci. USA* **108**, 6884–6888 (2011).
282. Faria, J. J., Dyer, J. R., Tosh, C. R. & Krause, J. Leadership and social information use in human crowds. *Animal Behav.* **79**, 895–901 (2010).
283. Bain, N. & Bartolo, D. Dynamic response and hydrodynamics of polarized crowds. *Science* **363**, 46–49 (2019).
284. Kim, M.-C., Silberberg, Y. R., Abeyaratne, R., Kamm, R. D. & Asada, H. H. Computational modeling of three-dimensional ECM-rigidity sensing to guide directed cell migration. *Proc. Natl Acad. Sci. USA* **115**, E390–E399 (2018).
285. Paluch, E. K. & Raz, E. The role and regulation of blebs in cell migration. *Curr. Opin. Cell Biol.* **25**, 582–590 (2013).
286. Tozluoglu, M. et al. Matrix geometry determines optimal cancer cell migration strategy and modulates response to interventions. *Nat. Cell Biol.* **15**, 751–762 (2013).
287. Moure, A. & Gomez, H. Three-dimensional simulation of obstacle-mediated chemotaxis. *Biomech. Model. Mechanobiol.* **17**, 1243–1268 (2018).
288. Besser, A. & Schwarz, U. S. Coupling biochemistry and mechanics in cell adhesion: a model for inhomogeneous stress fiber contraction. *New J. Phys.* **9**, 425–425 (2007).
289. Nishikawa, M., Naganathan, S. R., Jülicher, F. & Grill, S. W. Controlling contractile instabilities in the actomyosin cortex. *eLife* **6**, e19595 (2017).
290. Gross, P. et al. Guiding self-organized pattern formation in cell polarity establishment. *Nat. Phys.* **15**, 293–300 (2019).
291. Bratanov, V., Jenko, F. & Frey, E. New class of turbulence in active fluids. *Proc. Natl Acad. Sci. USA* **112**, 15048–15053 (2015).
292. Weber, C. A. et al. Long-range ordering of vibrated polar disks. *Phys. Rev. Lett.* **110**, 208001 (2013).

Acknowledgements
M.R.S., A.W. and H.R. acknowledge support by the Deutsche Forschungsgemeinschaft (DFG) within SFB 1027 (A3, A7). R.G.W. and G.G. acknowledge funding by DFG within the priority programme SPP 1726 "Microswimmers — from Single Particle Motion to Collective Behaviour".

Author contributions
All authors contributed to all aspects of manuscript preparation, revision and editing.

Competing interests
The authors declare no competing interests.

Publisher's note
Springer Nature remains neutral with regard to jurisdictional claims in published maps and institutional affiliations.

Supplementary information
Supplementary information is available for this paper at https://doi.org/10.1038/s42254-020-0152-1.